Quark–hadron duality in meson physics and quark confinement

V. V. Anisovich and A. V. Sarantsev
St. Petersburg Institute of Nuclear Physics, Gatching, Russia

Fiz. Élem. Chastits At. Yadra **27**, 5–52 (January–February 1996)

We investigate the concept of quark–hadron duality in meson physics at low and intermediate energies. Using a relativistic quark propagator that takes into account the confinement phenomenon and including scattering of pseudoscalar and vector mesons in the interaction dynamics, we have calculated the masses and widths of mesons that are S- and P-wave states of a quark–antiquark pair and also the meson–meson scattering amplitude up to energies $\sqrt{s}=1.3$ GeV. Our investigation has shown that the inclusion of pseudoscalar and vector mesons in the interaction dynamics leads to the following results: 1) The constituent quark mass is increased by about 200 MeV; 2) a barrier that is due to confinement forces and is responsible for the formation of highly excited states appears; 3) suppression of the instanton-induced forces that are needed in the construction of a purely quark model is observed. © *1996 American Institute of Physics.* [S1063-7796(96)00101-X]

1. INTRODUCTION

One of the most important problems in the physics of the strong interactions is the confinement of objects with color: quarks and gluons.[1,2] Intimately intertwined with this problem is the problem of calculating or explaining the properties of the constituent quark on the basis of the fundamental principles of quantum chromodynamics. This problem, which has always attracted the interest of physicists, has begun to be discussed particularly intensively in recent years.[3–6] It is a widely held view that the breaking of chiral symmetry responsible for the formation of constituent quarks is manifested at distances $r\simeq 0.1$–0.2 F. Thus, processes at large r can be described in terms of constituent quarks and effective gluons, both of which are very different from the quarks and gluons of chromodynamics.

Moreover, the success of the quark model in the description of the light hadrons has shown that at distances less than 1 F the constituent quarks can be regarded as ordinary particles, and therefore, when working with them, one can forget confinement. However, in the calculation of excited states and of the amplitudes of meson scattering at low and intermediate energies the confinement problem becomes a central one. Modeling of the confinement mechanism makes it possible to clarify different aspects of this phenomenon. In several papers devoted to hadron spectroscopy, confinement is modeled as an infinite potential wall (see, for example, Refs. 7–9). A qualitatively correct description of highly excited hadronic states was obtained with a linearly rising potential: $V(r)\sim \alpha r$ (see the discussions in Refs. 10–13). This shows that the confinement forces are not small at large distances and that the radius of the excited hadrons increases with their mass. However, the potential approach does not describe another important aspect of this phenomenon: Quarks can readily leave the confinement trap if their energy is sufficiently great for self-neutralization by means of the creation of a new quark–antiquark pair.

The phenomenon of soft quark neutralization was first discovered in the production of secondary particles in hadron interactions at high energies (see Ref. 14 and the references given there). In the fragmentation region, the produced particles carry the momenta of the spectator quarks of the initial hadron, and it is rather difficult to explain this effect in the model of a linearly rising quark potential or in the relativistic generalization of this model.

In this paper, we present a review of a series of investigations, individual results of which were published in Refs. 15–17 devoted to the construction of a relativistic confinement model on the basis of the transitions $q\bar{q}\to$mesons and $q\bar{q}\to$mesons$\to q\bar{q}$. Namely, these processes must form an effective "potential wall" responsible for the formation of the highly excited hadronic states. It is very probable that such a mechanism will also be able to clarify the phenomenon of quark–hadron duality, i.e., the possibility of describing the processes both in the language of hadrons and in the language of quarks. The best known and simplest example is $e^+e^-\to$hadrons annihilation. The total cross section $\sigma(e^+e^-\to\text{hadrons})$ is equal to the imaginary part of a quark single-loop diagram that has only a quark–antiquark threshold singularity. However, the unitarity condition is expressed in terms of hadronic and not quark singularities. This means that if we use the corresponding quark (or gluon) propagator, we can express the quark singularity in terms of a set of hadronic singularities. As will be shown in what follows, these hadronic singularities are intimately related to the constituent quark mass, and the establishment of this relationship is one of the central points of our investigation.

Thus, the construction of the confinement model is based on the following principles:

1) The quark propagators are defined in such a way that the quarks, bound by confinement forces, are not manifested in the form of free asymptotic states.

2) The quark diagrams that are used to calculate observable processes have the correct analytic properties—they correspond to hadronic singularities of the considered process.

To satisfy these requirements, it is convenient to use a spectral representation of the quark propagator expressed by means of an integral over the quark mass[18]—an analog of the Källén–Lehmann representation. In the framework of such

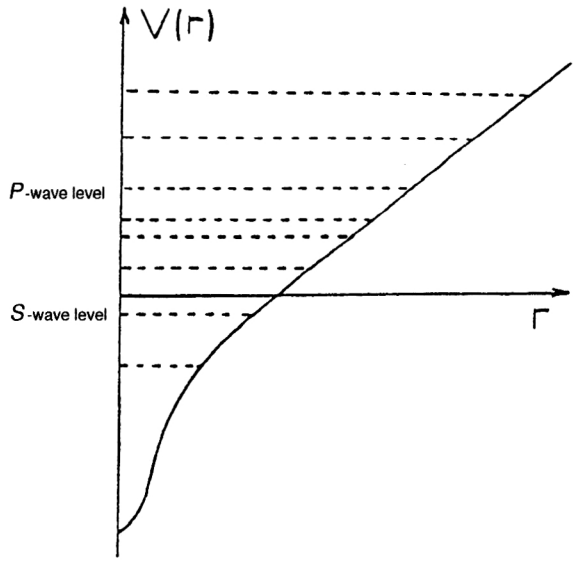

FIG. 1. Quark potential determined by the short-range interaction and the linearly rising confinement potential.

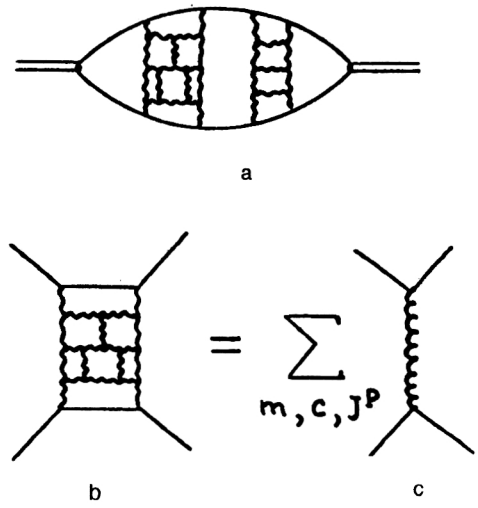

FIG. 2. a) Example of a planar diagram in the calculation of the meson self-energy part; b) interaction block of QCD gluons; c) diagram of the exchange of the effective particle.

an approach, we calculate the masses and widths of bound $q\bar{q}$ states: mesons with $J^P=0^-,1^-$ (S-wave $q\bar{q}$ states) and mesons with $J^P=0^+,1^+,2^+$ (P-wave $q\bar{q}$ states). Inclusion of $q\bar{q}\to$(two mesons) processes also makes it possible to calculate the scattering amplitudes of the pseudoscalar and vector mesons up to an energy $\sqrt{s}\leq 1.3$ GeV.

The constructed model has a number of features in common with approaches developed to describe mesons at low and intermediate energies. An example is the hybrid model of Ref. 19, in which not only quarks and gluons but also pions are included in the effective Lagrangian as Goldstone bosons. Meson–meson scattering amplitudes were calculated in Refs. 20 and 21 in the framework of a nonrelativistic quark model. The possibility of introducing mesonic degrees of freedom to describe highly excited states was discussed, for example, in Refs. 22–26.

The review is constructed as follows: In Sec. 2, we discuss without allowance for confinement the quark model that is the point of departure of our investigation. In Sec. 3, we consider the confinement mechanism, the method for taking this mechanism into account in the model, and the method of calculating the meson spectrum and meson–meson scattering amplitudes. The results of the calculations, the parameters used in the model, and their effect on the results of the calculations are discussed in Sec. 4. Brief conclusions are given in Sec. 5, and technical details are presented in three appendices.

2. DYNAMICAL QUARK MODEL WITHOUT ALLOWANCE FOR CONFINEMENT FORCES

Potential models, including relativistic generalizations of them, have helped to clarify many problems of meson spectroscopy. It is therefore appropriate to begin the discussion by using the results and language of the potential approach.

The standard version of the potential model is shown in Fig. 1. The potential responsible for the formation of the $q\bar{q}$ states can be divided into two regions: 1) the region of comparatively short distances (short-range forces) less than or of the order of 0.3–0.5 F; 2) the region of large distances (long-range forces) of the order of 1 F or more. The short-range part is determined mainly by an effective interaction of the type of gluon exchange and/or instanton-induced forces. The long-range part is usually parametrized by a linearly rising potential, $V(r)\sim ar$, and it is this part that is associated with the confinement forces (Refs. 27–30).

The short-range potential forces are responsible for the formation of the low-lying mesons, which are S-wave $q\bar{q}$ states with $J^P=0^-$ and 1^-. The long-range confinement forces are needed to construct the highly excited states of mesons with $J^P=1^+,2^+$, i.e., P-wave $q\bar{q}$ states and also other mesonic states (D-wave mesons, radial excitations, etc.). Especially mysterious are the 0^+ states, which are situated directly at the boundary between the two regions. The problem of the formation of these states requires special consideration.

In Ref. 15, we constructed a relativistic model of qq and $q\bar{q}$ interactions at low energy without allowance for the confinement forces, i.e., the quarks were treated as ordinary particles. The short-range component of the quark interaction was constructed as follows. The meson self-energy diagram due to the interaction of QCD quarks and gluons is considered. In accordance with the rules of the $1/N_c$ expansion, the main contribution to this process is made by planar diagrams of the type shown in Fig. 2a, in which the wavy lines denote QCD gluons. Diagrams of such type can be divided into interaction blocks and states with a propagating $q\bar{q}$ pair (for example, the diagram of Fig. 2a contains two interaction blocks and three intermediate $q\bar{q}$ states). The interaction block shown separately in Fig. 2b can be approximated by a sum of diagrams with the exchange of mesons and effective colored particles (see Fig. 2c). In this case, the amplitude of the block in Fig. 2b, which we denote by V, is equal to the sum of the propagators of effective particles with different masses, colors, total angular momentum, and parity (m,c,J^P):

$$V=\sum_{m,c,J^P} B_{m,c,J^P}(s)d_{m,c,J^P}(t),$$

where

$$d_{m,c,J^P}\sim(m^2(c,J^P)-t)^{-1}. \tag{1}$$

The amplitude V is a function of the square of the total energy s and of the square of the momentum transfer t. If we restrict consideration to the interaction of quarks in the low-energy region, then the factor $B_{m,c,J^P}(s)$ can be assumed to depend weakly on s, and the calculation of the interaction can be restricted to the contribution of the states with lowest J^P. Calculations of the quark model show that exchange of an effective gluon with comparatively large mass and the quantum numbers of a QCD gluon is most important. Such an interaction leads to chromomagnetic forces that give a qualitatively correct splitting of the $SU(6)$ multiplet.[7,31] However, for the quantitative description of the pion mass and the splitting of the $\eta-\eta'$ mesons, it is necessary to introduce in addition a white interaction with quantum numbers $J^P=0^-$. A good candidate for such an interaction is provided by instanton-induced forces.

We now consider the significance of the appearance of an effective gluon mass from the point of view of the effective phenomenological Lagrangian that describes the soft processes. Such a Lagrangian must be constructed on the basis of the QCD Lagrangian and, therefore, must be renormalizable, like the Lagrangian of the original theory. In addition, the effective Lagrangian must possess global color symmetry. One of the natural ways of breaking local color symmetry of the QCD Lagrangian while preserving global symmetry is spontaneous breaking realized by the introduction of three colored triplets of Higgs fields.[32,33] Such breaking leads to the appearance of an effective massive gluon and ten scalar particles (for example, an octet of colored and two white Higgs bosons). The parameters of the model can be chosen in such a way that if the composite gluon has mass ~700 MeV, the masses of the Higgs bosons are in the range 1–1.5 GeV. Thus, such a model[32] contains not only quark–antiquark bound states but also in the scalar sector two white Higgs bosons in the range 1–1.5 GeV and glueballs with mass in the range 1.4–1.9 GeV. Despite the apparent excessive number of exotic states, such a model does not contradict present experimental data—the number of bound states found in the scalar sector (see, for example, Refs. 33 and 34 and the review[35] of the Particle Data Group) significantly exceeds the number of states predicted by the $q\bar{q}$ systematics.

An iterative bootstrap procedure is used in Ref. 15 to calculate the quark–antiquark bound states. Two types of forces are introduced as the initial interaction: i) exchange of an effective gluon; ii) an instanton-induced interaction. Both types of forces are parametrized as a four-point interaction:

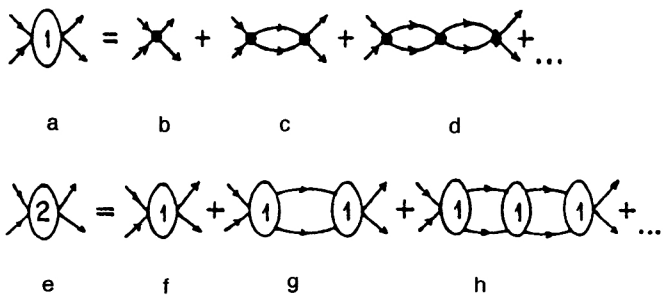

FIG. 3. Diagrams calculated in the iterative procedure: a) diagrams of the first iteration, equal to a sum of diagrams (b,c,d). Diagrams of the second iteration, in the calculation of which the diagrams of the first iteration are used as "forces" in the s, t, and u channels (f, g, h, etc.).

$$\begin{aligned} &g_V^{(qq)}(\bar{q}\boldsymbol{\lambda}\gamma_\mu q)^2+2g_V^{(qs)}(\bar{q}\boldsymbol{\lambda}\gamma_\mu I_f q)(\bar{s}\boldsymbol{\lambda}\gamma_\mu s)+g_V^{(ss)}(\bar{s}\boldsymbol{\lambda}\gamma_\mu s)^2\\ &+\tfrac{1}{2}\tilde{g}_I(\bar{q}(1+\gamma_5)I_f q)^2-\tfrac{1}{2}\tilde{g}_I(\bar{q}(1+\gamma_5)\boldsymbol{\tau}_f q)^2\\ &-2\tilde{g}_S(\bar{s}(1+\gamma_5)q)(\bar{q}(1+\gamma_5)s)\\ &+\tilde{g}_S(\bar{s}(1+\gamma_5)s)(\bar{q}(1+\gamma_5)q). \end{aligned} \tag{2}$$

Here $\boldsymbol{\tau}$ are the isotopic Pauli matrices, $\boldsymbol{\lambda}$ are color matrices, q is an isotopic column of bispinors of nonstrange quarks, and s is the bispinor of the strange quark. The coefficient g_V characterizes the strength of the forces due to the exchange of the effective gluon, and the coefficients $\tilde{g}_I$ and $\tilde{g}_S$ characterize the instanton interaction in the nonstrange and strange sectors. The breaking of the flavor $SU(3)$ symmetry is parametrized in the form

$$g_V=\frac{m_q^2}{\pi^2}\,g_V^{(qq)}=\frac{(m_q+m_s)^2}{4\pi^2}\,g_V^{(qs)}=\frac{m_s^2}{\pi^2}\,g_V^{(ss)},$$

$$g_I=\frac{m_q^2}{\pi^2}\,\tilde{g}_I,\quad g_S=\frac{m_q m_s}{\pi^2}\,\tilde{g}_S. \tag{3}$$

The mass of the nonstrange quark, m_q, is taken to be 385 MeV, and the mass of the strange quark, m_s, is 510 MeV. To eliminate the divergence in the single-loop quark diagrams, the single-loop integral is regularized by means of the cutoff function

$$F(\Lambda,s,m_1,m_2)=\exp\left[-\Lambda\left(\frac{s}{(m_1+m_2)^2}-1\right)\right]. \tag{4}$$

Here Λ is the cutoff parameter, s is the square of the total energy of the quark–antiquark pair in the dispersion representation of the loop diagram, and m_1 and m_2 are the quark and antiquark masses. We note that investigation of the model revealed it to be insensitive to the form of parametrization of the cutoff function. For example, the use of the θ function or a function with power-law decrease in s gives very similar results.

The scattering amplitude obtained after the first iteration (Fig. 3a) is equal to the sum of the diagrams shown in Figs. 3b, 3c, and 3d, in which the point vertex is determined by the interaction (2). The four parameters g_V, g_I, g_S, and Λ of the model are fixed by the experimental masses of the π, K, η', and ρ mesons. An iterative bootstrap procedure is then used. This means that the calculated amplitudes are used as the

TABLE I. Masses and partial widths of $J^{PC}=0^{-+}$ and $J^{PC}=1^{--}$ mesons. All quantities are given in mega-electron-volts.

Calculated quantity	$m_q=390$ $\Delta=0$	$m_q=625$ $\Delta=0$	$m_q=625$ $\Delta=100$	$m_q=625$ $\Delta=200$	Experiment
$m(\pi)$	140	140	140	140	140
$m(K)$	495	495	495	495	495
$m(\eta)$	550	562	564	565	548
Θ_P(deg)	−18	−10	−10	−10	−10 to −20
$m(\eta')$	960	960	960	960	958
$m(\rho)$	770	775	775	775	768
$\Gamma_{\pi\pi}$	-	150	150	150	149±3
$m(K^*)$	890	886	885	885	892
$\Gamma_{K\pi}$	-	48	48	50	50±1
$m(\omega)$	765	767	766	766	782
$\Gamma_{3\pi}$	-	-	-	-	8
$m(\Phi)$	1025	1044	1046	1048	1020
Γ_{KK}	-	4	4	5	4.5

initial interaction in the following iteration (see Figs. 3f, 3g, and 3h). The interaction parameters were determined in such a way as to recover the correct masses of the above mesons. Such an iterative procedure converges comparatively rapidly—usually two iterations are entirely sufficient (five iterations were performed in order to test the convergence).

The results of the calculations are presented in the first columns of Tables I and II. It can be seen that the masses and mixing angles of the η, ω, K^*, and Φ mesons agree satisfactorily with the experimental data. This is an indication that in the calculation of the properties of the low-lying mesons the confinement forces can be ignored. Moreover, the scalar mesons obtained in the model have masses of about 1000 MeV. This is an important result, and we shall discuss it below in more detail.

Another interesting result concerns the mass of the composite gluon. As the initial interaction of the iterative procedure we used the Lagrangian (2) in which the interaction of gluon type is a point interaction, corresponding to an infinite effective mass of the composite gluon. However, after completion of the iterative procedure with allowance for $G_{\text{eff}}\to q\bar{q}\to G_{\text{eff}}$ transitions a composite gluon with finite mass $M_G\sim 700$ MeV is obtained. This value is fairly stringently related to the mass of the ρ meson, which was used to fix the parameters. We consider this phenomenon in more detail, using the language of potential interaction (however, it must be borne in mind that such an interpretation gives only a very crude reflection of the results of the bootstrap approach, which is a relativistic method that takes into account the interaction dynamics in the crossed channels). The effective potential equivalent to the bootstrap interaction is shown schematically in Fig. 4a. This potential corresponds to the short-range part of the potential in Fig. 1 (i.e., the long-range part directly related to the confinement forces at $r>1$ F is absent). The mean range of the potential in Fig. 4 is mainly determined by the reciprocal of the composite gluon: $\langle r\rangle_{\text{well}}\sim 1/M_G$. On the other hand, this same range is determined by the meson masses chosen to fix the parameters. It is this that has the consequence that the gluon mass is close to the mass of the ρ meson. For such a mass of the composite gluon, the mass of the lowest glueball ($J^{PC}=0^{++}$) must be about $2M_G\sim 1400$ MeV. This value is very close to the value

TABLE II. Masses and partial widths of $J^{PC}=0^{++}$ mesons. The resonance mass is defined as the position of the maximum in the square of the scattering amplitude. All quantities are given in mega-electron-volts.

Calculated quantity	$m_q=390$ $\Delta=0$	$m_q=625$ $\Delta=0$	$m_q=625$ $\Delta=100$	$m_q=625$ $\Delta=200$	Experiment
$m(f_0)$	780	875	877	875	880±20
$m(a_0)$	950	998	998	998	985
Γ_{tot}	-	84	76	70	57±11
$\Gamma_{K\bar{K}}$	-	72%	75%	73%	seen
$\Gamma_{\pi\eta}$	-	28%	25%	27%	seen
$m(K_0)$	1080	1250	1242	1236	1430±6
Γ_{tot}	-	300	316	320	287±23
$\Gamma_{K\pi}$	-	88%	84%	87%	93%
$\Gamma_{K\eta}$	-	12%	16%	13%	-
$m(f_0)$	1200	1715	1718	1720	1710±5
Γ_{tot}	-	144	190	230	150±15
$\Gamma_{q\bar{q}}$	-	18%	18%	17%	-
$\Gamma_{s\bar{s}}$	-	48%	48%	50%	-
$\Gamma_{K\bar{K}}$	-	22%	21%	21%	seen
$\Gamma_{\pi\pi}$	-	8%	7%	7%	-
$\Gamma_{\eta\eta}$	-	4%	6%	7%	-

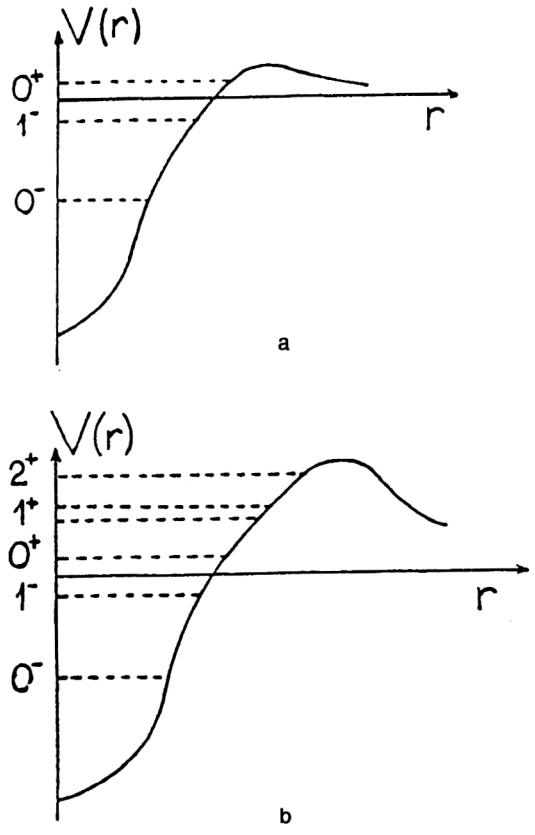

FIG. 4. a) Potential corresponding to the forces used in the model without confinement. b) The potential after inclusion of the meson box diagram.

obtained according to the mechanism of the quenched approximation[39,40] of lattice QCD, in which the mass of the lowest glueball is $m_{\text{glueball}}(0^{++})\sim 1550$ MeV (Ref. 41).

Note that the bootstrap quark model without allowance for confinement forces correctly gives the other low-energy quantities, for example, the nucleon and Δ-isobar masses and the pion and kaon form factors.[15,42]

We summarize the main results of the model considered above:

1) This model gives a very good description of the short-range part of the interaction, where the exchange of a composite gluon with mass 700 MeV plays the central role. The instanton forces are weak compared with the gluon forces, $g_V/g_I\sim 1/4$, but they are needed to explain the gluon mass and to obtain the correct splitting and mixing angle of the $\eta-\eta'$ mesons.

2) The scalar mesons have a mass of about 1 GeV.

3. THE $q+\bar{q}\to M+M$ TRANSITION AS THE PROCESS RESPONSIBLE FOR THE CONFINEMENT MECHANISM

In the previous section, we considered an iterative bootstrap model, in the framework of which the short-range component of the quark-interaction forces was investigated. The next step is the construction of the long-range component—the confinement forces. In the potential models, this problem is solved by means of a linearly rising potential barrier: $V\sim\alpha r$. This potential barrier must ensure two main properties of confinement: the formation of highly excited bound states and the absence of asymptotically free quarks. Although the first property is very satisfactorily fulfilled (the spectrum obtained in the potential models agrees well with the experimental data), the fulfillment of the second property in this approach leaves many open questions. In reality, confinement forces should not act as an absolutely impenetrable barrier: the majority of excited hadrons decay readily into multihadron states; therefore, the production of an additional quark–antiquark pair readily ensures color neutralization. Figure 5a shows an example of such a process: The quarks that form an excited $q\bar{q}$ state are emitted, producing a new

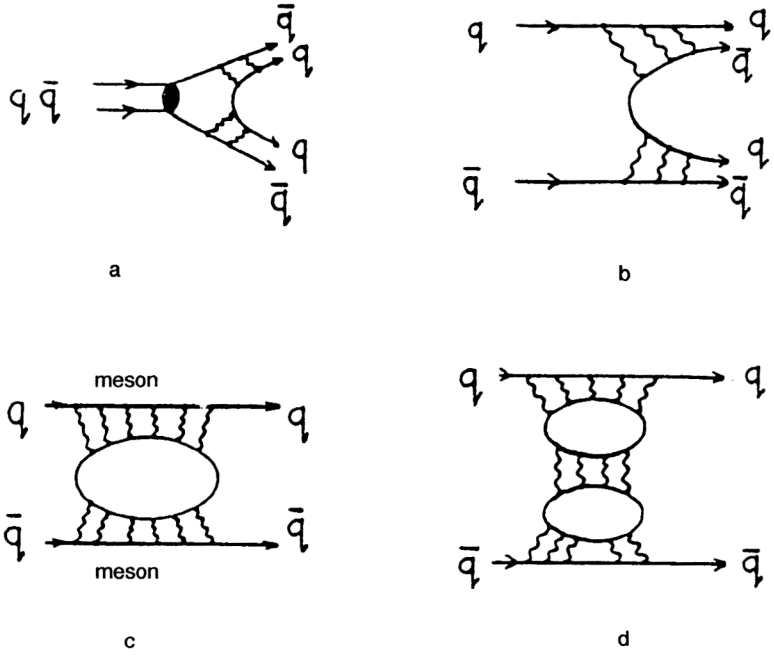

FIG. 5. a), b) Diagrams corresponding to quark deconfinement; c), d) meson box diagrams responsible for formation of the confinement barrier.

quark–antiquark pair and thus forming two outgoing mesons. Such a transition, which we shall denote by $q+\bar{q}\to MM$, is shown separately in Fig. 5b; it plays the main role in confinement physics.

The importance of the process shown in Fig. 5b was recognized quite a long time ago. Moreover, investigation of the secondary particles in the fragmentation region in high-energy collisions of hadrons supplies direct information about the "soft" production of new quark–antiquark pairs: The momentum distribution of the spectator quark is repeated with good accuracy in the distribution of the secondary particles (see Ref. 14 and the references given there).

The process of transition of a quark–antiquark pair into mesons is the main object of our investigation. If we investigate only quark–antiquark transitions, then the box diagram shown in Fig. 5c corresponding to the product of two $q+\bar{q}\to M+M$ amplitudes determines the confinement forces at $r\geqslant 1$ F. In other words, the diagram of Fig. 5c must create a potential barrier for the first excited states of the type of Fig. 4b if low-lying mesons form the intermediate states in the box diagram. It may be hoped that the set of diagrams shown in Figs. 5c, 5d, etc., is capable of reproducing the entire "barrier" that determines the confinement forces. On the other hand, all these diagrams have an imaginary part due to meson production and, therefore, reflect another aspect of confinement: the process of soft color neutralization.

4. QUARK–HADRON DUALITY

Allowance for the box diagram of Fig. 5c does not prevent quarks from leaving the interaction region in the form of asymptotically free particles. Therefore, it is necessary to take a further step and modify the quark propagator.

Modification of the quark propagator to ensure quark behavior as $|r|\to\infty$ as an exponentially damped wave has long attracted attention. Propagators that contain only poles in the complex plane of k^2 can give such damping, and the simplest diagrams, for example, the single-loop quark diagram, will not contain any quark singularities on the first physical sheet. However, the existence of quark singularities in more complicated quark diagrams remains an open question. In any case, such an approach contains a serious shortcoming—quark–hadron duality is not in any way taken into account. One of the methods that makes it possible to take into account this property is use of the Källén–Lehmann representation for the description of the quark propagator:

$$\mathcal{G}(k)=\int_{\mu^2}^{\infty} dm^2\rho(m)\,\frac{1}{m-\hat{k}}, \tag{5}$$

where $\rho(m)$ is the distribution of the quark mass and has properties that will be discussed subsequently. We note immediately that this representation should not be regarded literally as the propagator of an individual free quark; it mainly reflects the properties of a quark in the quark–antiquark interaction.

The well-known process $e^+e^-\to$hadrons gives an example of quark–hadron duality, in which the imaginary part of the single-loop quark diagram corresponds to the sum of the imaginary parts of the hadron diagrams. We shall consider this process in more detail. The single-loop quark diagram describing the process $\gamma^*\to q\bar{q}\to\gamma^*$ (Fig. 6a) is

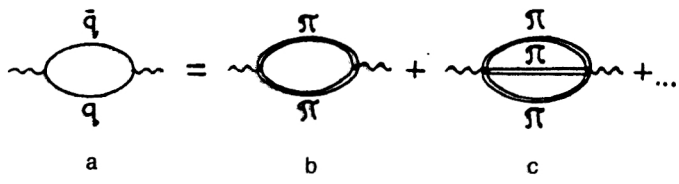

FIG. 6. a) Single-loop $q\bar{q}$ diagram; b), c) the corresponding meson diagrams.

$$\Pi_{q\bar{q}}^{\nu\nu'}=-N\int_{\mu^2}^{\infty}dm_1^2\rho(m_1)\int_{\mu^2}^{\infty}dm_2^2\rho(m_2)$$
$$\times\int\frac{d^4k}{i(2\pi)^4}\,\mathrm{Tr}\left\{\Gamma_\nu\frac{1}{m_1-\hat{k}_1}\Gamma_{\nu'}\frac{1}{m_2-\hat{k}_2}\right\}, \tag{6}$$

where ν,ν' are photon indices, and N is the number of colors (we consider a diagram for a fixed quark flavor). For the imaginary part of this amplitude, we obtain the expression

$$\mathrm{Im}\,\Pi_{q\bar{q}}^{\nu\nu'}(p)=N\int_{4\mu^2}^{(m_1+m_2)^2\leqslant s}dm_1^2dm_2^2\rho(m_1)\rho(m_2)$$
$$\times\Phi(s,m_1,m_2)\int\frac{d\Omega_{\mathbf{k}}}{4\pi}\,\mathrm{Tr}\{\Gamma_\nu(m_1+\hat{k})\Gamma_{\nu'}(m_2+\hat{k}-\hat{p})\}, \tag{7}$$

where p is the photon momentum, $s=p^2$, and $\Phi(s,m_1,m_2)$ is the two-particle phase space:

$$\Phi(s,m_1,m_2)=\frac{1}{16\pi s}\times\sqrt{[s-(m_1+m_2)^2][s-(m_1-m_2)^2]}. \tag{8}$$

Integration over the solid angle $d\Omega_{\mathbf{k}}$ is integration over all directions of the vector $\mathbf{k}$ for fixed values of the 4-vectors k and $p-k$, namely $k^2=m_1^2$ and $(p-k)^2=m_2^2$. The integration over the quark masses is restricted by the condition $2\mu\leqslant m_1+m_2\leqslant\sqrt{s}$. For $\sqrt{s}\leqslant 2\mu$, this leads to the equation

$$\mathrm{Im}\,\Pi_{q\bar{q}}^{\nu\nu'}=0. \tag{9}$$

The total cross section the annihilation of $e^+e^-\to$hadrons is proportional to the imaginary part of the amplitude (7):

$$\Pi_{q\bar{q}}^{\nu\nu'}(s)=(-p^2\delta_{\mu\nu}+p_\mu p_\nu)\Pi(s),$$
$$\sigma(e^+e^-\to\text{hadrons})\sim\sum_{\text{color}}\mathrm{Im}\,\Pi(s). \tag{10}$$

The experimentally observed processes are $e^+e^-\to 2\pi$, $e^+e^-\to 3\pi$, etc. These processes are determined by the imaginary part of the diagrams shown in Figs. 6b, 6c, etc. Thus, we obtain the correspondence

$$\sum_{\text{color}}\mathrm{Im}\,\Pi_{q\bar{q}}^{\nu\nu'}(s)=\mathrm{Im}\,\Pi_{2\pi}^{\nu\nu'}(s)+\mathrm{Im}\,\Pi_{3\pi}^{\nu\nu'}(s)+\ldots, \tag{11}$$

where the sum on the right-hand side of the equation includes all the hadronic contributions to the self-energy parts. Equation (11) is the duality condition for the single-loop quark diagram when gluon emission is ignored. It can be seen that in Eqs. (5)–(7) we must set $\mu=\mu_\pi$, since the first process of hadron production that is allowed energetically is the process $e^+e^-\to 2\pi$.

As we have already noted, the right-hand side of Eq. (11) contains only hadron singularities; this reflects the fact that the observable particles are the hadrons and not the quarks. Thus, the single-loop quark diagram [the left-hand side of Eq. (11)] must contain the same hadron singularities. This means that the integration over the mass of the quarks must not only annihilate the quark singularities but also introduce corresponding hadron singularities. In reality, Eq. (11) can be regarded as an equation that determines the distribution of the quark mass. It makes it possible to reconstruct the singularities of $\rho(m)$, for example, the singularity at $s=9\mu_\pi^2$ (the threshold singularity corresponding to 3π production) corresponds to a singularity in $\rho(m)$ at $m=2\mu_\pi$.

Extension of Eq. (6) to the region of high energies leads to the result of perturbative QCD. Indeed, in the strongly virtual region, it is possible to ignore the quark mass in the propagator [i.e., make the substitution $(m-\hat{k})\to(-\hat{k})$] and thus reduce Eq. (6) to the normal expression in QCD:

$$\Pi_{q\bar{q}}^{\nu\nu'}(p)=-N\int\frac{d^4k}{i(2\pi)^4}\,\mathrm{Tr}\left\{\Gamma_\nu\frac{1}{-\hat{k}_1}\Gamma_{\nu'}\frac{1}{-\hat{k}_2}\right\},\quad(12)$$

provided that there is fulfillment of the normalization condition

$$\int_{\mu^2}^{\infty}dm^2\rho(m)=1.\quad(13)$$

Thus, the representation of the quark propagator in the form of the spectral integral (5), first proposed in Ref. 18, does not destroy the transition to the high-energy limit and simultaneously generates in the region of soft QCD the correct singularities of the scattering amplitude on the real axis at $s>4\mu_\pi^2$, making it possible to satisfy directly the requirement of quark–hadron duality. Integration over the quark masses removes the quark singularities in the scattering amplitude from the first physical sheet and introduces new singularities corresponding to real hadronic states. This is the key point in the fulfillment of Principles 1 and 2 formulated in the Introduction.

Experience of working with the quark model has shown that the distribution function ρ can be chosen to be independent of the type of reaction and to be strongly localized around a definite mass. In the considered model, we chose the following parametrization of this function:

$$\rho(m)=\frac{C\sqrt{m^2-\mu^2}}{(m^2-m_0^2)^2+\Delta^4},\quad(14)$$

where μ is equal to the pion mass for the nonstrange quarks and to the kaon mass for the strange quarks, and C is a normalization constant determined by Eq. (13). For a narrow distribution, $\Delta\ll m_0$, the dimensional quantity m_0 plays the role of a constituent quark mass.

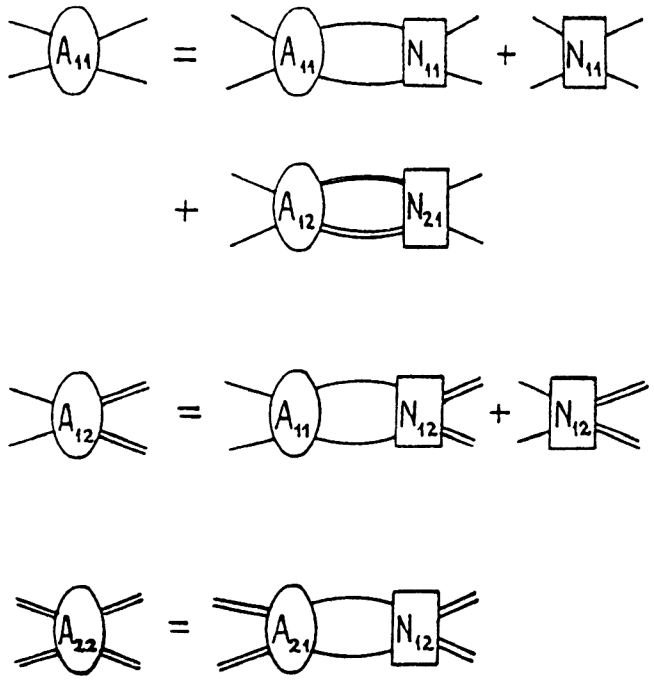

FIG. 7. The Bethe–Salpeter equation in the case of coupled quark–antiquark and meson channels.

5. BETHE–SALPETER EQUATION FOR THE MESON SCATTERING AMPLITUDE

As was discussed in the previous section, the interaction of the constituent quarks effectively takes into account the contribution of all the hadronic states allowed in the given channel. Let us consider what happens to the $q\bar{q}$ interaction if we take into account some of these hadronic channels explicitly—as additional channels to $q\bar{q}$. To calculate the meson spectrum and meson–meson scattering amplitudes in this case, we shall use the Bethe–Salpeter equation shown graphically in Fig. 7. Here and in what follows, we use the index 1 for the $q\bar{q}$ state and the index 2 for the two-meson state. Thus, for the partial-wave amplitude with quantum numbers J^P (index j) the block A_{11}^j describes the transition amplitude $q\bar{q}\to q\bar{q}$, the block A_{12}^j describes the transition $q\bar{q}\to MM$, and the block A_{22}^j describes the $MM\to MM$ amplitude. As the initial interaction we have introduced a direct quark–antiquark interaction characterized by the function N_{11} and a $q\bar{q}\to MM$ transition characterized by the function N_{12}.

We recall that in the bootstrap quark model of Ref. 15 the $q\bar{q}\to MM$ transition was not taken into account, and therefore just one equation for A_{11}^j, without a meson loop, was solved. The total quark–antiquark interaction must contain two parts: a short-range interaction and a long-range interaction (confinement forces). In Ref. 15, only the short-range component was taken into account, and we hope to take into account an appreciable fraction of the long-range component by means of appropriate single-loop meson diagrams. In order to see more clearly the contribution of the meson diagrams to the quark–antiquark interaction, we substitute the equation for A_{12}^j in the equation for the block A_{11}^j.

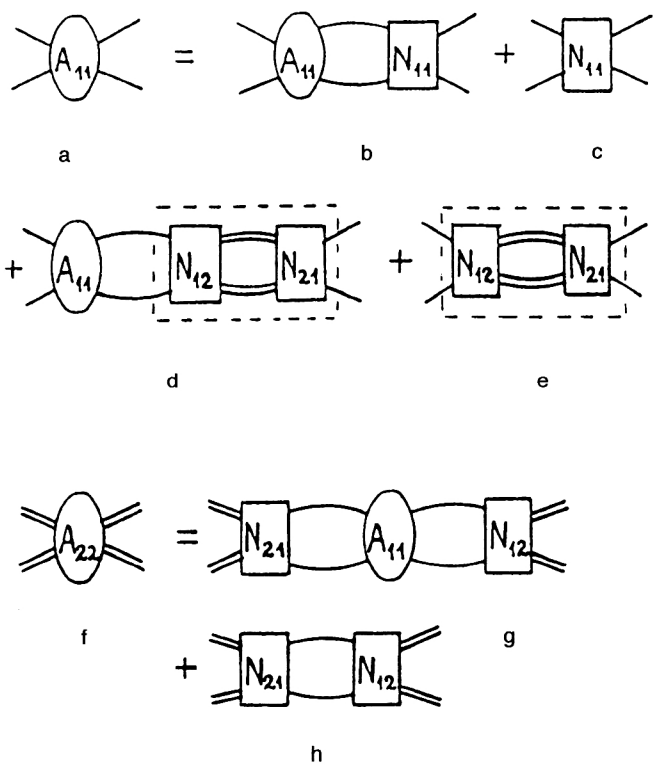

FIG. 8. The Bethe–Salpeter equation with meson box diagrams as the effective $q\bar{q}\to q\bar{q}$ interaction.

The equations then obtained for A^j_{11} and A^j_{22} are shown in graphical form in Fig. 8.

When the equation is expressed in such a form, it can be clearly seen that the effective $q\bar{q}\to q\bar{q}$ interaction in our model consists of two parts: a part due to the direct quark–antiquark interaction (Fig. 8c) and a part due to a box diagram with two mesons in the intermediate state (Fig. 8e). The first part corresponds to short-range forces and is chosen in the same form as in Ref. 15: It is parametrized by instanton-induced forces and the exchange of an effective gluon. The second part models the confinement forces but, of course, has a much more complicated structure than the linearly rising potential barrier in the nonrelativistic approach. The interaction described by the meson box diagrams has an imaginary part determined by transition to the two-meson state. Note that although the $q\bar{q}\to MM$ transition can be parametrized in a fairly simple form, the effective $q\bar{q}\to q\bar{q}$ interaction, which is equal to the sum of box diagrams with different mesons in the intermediate state, has a very complicated structure.

When several meson channels are taken into account explicitly, it is obvious that not only the parameters of the quark–antiquark interaction must be redetermined (compared with Ref. 15) but also the properties of the quark propagator. If we take into account explicitly the scattering channels of the lowest mesons (for example, the S-wave $q\bar{q}$ states 0^- and 1^-), then the mean mass m_0 in the distribution function $\rho(m)$ is shifted to larger values, and the distribution itself becomes broader. This arises from the fact that when explicit allowance is made for the lowest two-meson channels the quark–antiquark channel is related by a duality condition only to the scattering channels of heavier mesons and to multimeson scattering channels. With the renormalized quark propagator and with allowance for the two-particle scattering channels of the lowest mesons, it is necessary to reproduce the spectrum of the lowest mesons (self-consistency condition) and simultaneously obtain the excited mesonic states (such as P-wave $q\bar{q}$ states). After this, the procedure can be repeated with explicit allowance for the scattering channels of these P-wave mesons and, therefore, with a new redetermination of the quark propagator in order to calculate even higher mesonic states (for example, radial excitation of S-wave mesons), and so on. One of the main ideas in the creation of such a model is also the possibility of reproducing the effective confinement interaction on the basis of a simple initial interaction and taking into account, step by step, more and more mesonic degrees of freedom explicitly.

At the first glance, the structure of the decay of the highly excited mesons obtained at the intermediate step of our model is rather unusual: On the one hand, there exists a transition of a highly excited meson to a real two-meson state, $M^*\to MM$, while, on the other hand, the amplitude can still contain an "unphysical" transition $M^*\to q\bar{q}$. The total decay width of such a meson is equal to the sum of these widths. The physical interpretation of the width of decay to the $q\bar{q}$ state is that it reflects decays of a highly excited state into hadronic states that are not taken into account explicitly, for example, into multimeson states. It is expected that when allowance is made for a large number of mesonic states explicitly and, accordingly, there is a shift of the effective quark mass the partial width of the transition to the $q\bar{q}$ state will be decreased until it disappears completely (and the considered model goes over into a meson model of one of the types proposed in Refs. 43 and 44).

After this general discussion, we turn to the calculation of specific amplitudes. For this, we consider the structure of the matrix elements in the Bethe–Salpeter equation for fixed quantum numbers J^P (characterized by an index j). This structure can be written in the form

$$(\bar{\psi}_2 Q^B_j \psi_1) A^j_{11} (\bar{\psi}_3 Q^B_j \psi_4),$$
$$(\bar{\psi}_2 Q^B_j \psi_1) A^j_{12} (\varphi^A_3 * O^{ABC}_j \varphi^C_4),$$
$$(\varphi^A_2 * O^{ABC}_j \varphi^C_1) A^j_{22} (\varphi^D_3 * O^{DBE}_j \varphi^E_4), \qquad (15)$$

where ψ_i are the spinors of the fermions in the initial and final states, φ^A are the boson wave functions, and Q^B_j and O^{ABC}_j are fermion and boson partial operators in channel j. The multi-indices A,B,C,D,E characterize both the vector structure of the operators and the polarizations of the bosons.

The operators Q^B_j and O^{ABC}_j can be constructed by means of the orthogonality condition for the imaginary part of the single-loop diagram at an energy above the threshold of constituent production:

1) for the fermion (quark–antiquark) channel

$$\int \frac{d^4k}{i(2\pi)^4} \mathrm{Tr}\{Q^C_i(m_1+\hat{k})Q^B_j(m_2+\hat{k}-\hat{P})\}\delta(m_1^2 - k^2)\delta(m_2^2-(P-k)^2) = \delta_{CB}\delta_{ij}\Phi^1_j(s,m_1,m_2); \qquad (16)$$

2) for the boson channel (two pseudoscalar mesons, a pseudoscalar meson and a vector meson or two vector mesons)

$$\int \frac{d^4k}{i(2\pi)^4} O_i^C O_j^B \delta(\mu_1^2-k^2)\delta(\mu_2^2-(P-k)^2) = \delta_{CB}\delta_{ij}\Phi_j^2(s,\mu_1,\mu_2), \quad (17)$$

$$\int \frac{d^4k}{i(2\pi)^4} O_i^{C\Lambda}\left(g_{AD}-\frac{k_A k_D}{\mu_1^2}\right) O_j^{DB}\delta(\mu_1^2-k^2)\delta(\mu_2^2-(P-k)^2) = \delta_{CB}\delta_{ij}\Phi_j^2(s,\mu_1,\mu_2), \quad (18)$$

$$\int \frac{d^4k}{i(2\pi)^4} O_i^{ACD}\left(g_{DE}-\frac{k_D k_E}{\mu_1^2}\right) O_j^{EBF}\left(g_{FA}-\frac{(P-k)_F(P-k)_A}{\mu_2^2}\right)\delta(\mu_1^2-k^2)\delta(\mu_2^2-(P-k)^2) = \delta_{CB}\delta_{ij}\Phi_j^2(s,\mu_1,\mu_2). \quad (19)$$

The functions Φ_j^1 and Φ_j^2 are the phase spaces for the two-fermion and two-boson scatterings in the state j, δ_{ij} is the Kronecker delta symbol for states with different J^P, and g_{ab} is the metric tensor.

Such a definition of orthogonality is particularly convenient when one is using the dispersion technique to calculate the diagrams: In this case, vanishing of the imaginary part of a single-loop diagram of a transition between different states automatically leads to vanishing of the real part of such a transition as well. The list of fermion and boson operators Q_j^C, O_j^{ABC} and the expressions for the phase spaces $\Phi_j^i(s)$ for scattering of fermions and pseudoscalar and vector bosons is given in Appendix A.

To calculate the single-loop diagrams, it is convenient to use the technique of dispersion integration. This technique is relativistically invariant and is relatively simple in the case of the calculation of amplitudes that have several scattering channels; this is very important for the given model. A dispersion technique for integrating with respect to the mass of a composite particle was developed in Refs. 45 and 46, where it was applied to the description of the two-nucleon system and demonstrated its ability to give an adequate description of both the scattering amplitudes and the properties of the bound state. This technique is natural for taking into account meson scattering channels, but the question arises of the possibility of using this technique for quarks and gluons: These particles never manifest themselves as free asymptotic states. We note first of all that such a problem exists not only when the dispersion technique is used but also in any relativistic approach to the interaction of colored objects, for example, when one uses Feynman diagrams or light-cone variables (a detailed comparison of these three approaches can be found in Ref. 47). A general problem that arises irrespective of the technique that is used can be formulated in the language of the singularities of the amplitudes: The amplitudes of observable processes on the first physical sheet must contain only hadronic singularities. The use of a spectral representation with respect to the quark mass solves this problem: In the first stage, one can regard the quarks as real particles and, therefore, use any technique to calculate the quark diagrams; then, having integrated over the quark masses, one can remove the quark singularities from the first sheet, introducing corresponding hadron singularities in place of them.

Thus, to calculate the meson spectrum and the meson–meson scattering amplitudes, the following scheme is used.

1. In the first stage, the quarks are treated as asymptotically free particles but with different masses in the initial, final, and intermediate states. The technique of dispersion integration is used to solve the Bethe–Salpeter equation. The transition from the Bethe–Salpeter equation expressed in the language of Feynman diagrams to an equation expressed in the language of dispersion integration is given in Ref. 47. In the dispersion approach, both the interaction kernel N_{ik}^j (containing only left-hand singularities of the partial-wave amplitude) and the partial amplitude A_{ik}^j itself (where i, $k=1$, 2 and $j=J^P$) depend on two parameters: the squares of the total energy of the two particles in the initial and final states, which we shall denote by s and s', respectively. The expression for the Bethe–Salpeter equation, expressed in the framework of the dispersion technique, has the form

$$\begin{aligned}
A_{11}(s,s_1) &= \int \frac{ds'}{\pi} A_{11}^j(s,s') \times \frac{\Phi_j^1(s',m_1,m_2)N_{11}^j(s',s_1)}{s'-s} + \int \frac{ds'}{\pi} \times A_{12}^j(s,s') \frac{\Phi_j^2(s',\mu_1,\mu_2)N_{21}^j(s',s_1)}{s'-s} + N_{11}^j(s,s_1),\\
A_{12}^j(s,s_1) &= \int \frac{ds'}{\pi} A_{11}^j(s,s') \times \frac{\Phi_j^1(s',m_1,m_2)N_{12}^j(s',s_1)}{s'-s} + N_{12}^j(s,s_1),\\
A_{22}^j(s,s_1) &= \int \frac{ds'}{\pi} A_{12}^j(s,s') \frac{\Phi_j^1(s',m_1,m_2)N_{21}^j(s',s_1)}{s'-s}.
\end{aligned} \quad (20)$$

It is convenient to solve this equation under the assumption of factorization of the kernels $N_{ik}(s,s')$ in the form of a sum of products of vertices G_{ik}^m containing, like the kernel, only left-hand singularities of the partial scattering amplitude [to simplify the expressions, we omit in Eqs. (21)–(23) the index that characterizes J^P]:

$$N_{ik}(s,s') = \sum_m G_{ik}^m(s)G_{ki}^m(s'). \quad (21)$$

In this case, the Bethe–Salpeter equation can be rewritten in the form

$$A_{ik}(s,s') = \sum_{mp} G_{ip}^m(s)a_{ipk}^m(s'),$$

$$a_{ipk}^m = \sum_{nl} a_{ilp}^n B_{lpk}^{nm} + G_{ik}^m\delta_{ip}, \quad (22)$$

where α^m_{ipk} is the interaction block that characterizes the transition from state i to the state with right vertex G^m_{pk} in the final single-loop diagram. The single-loop function is

$$B^{nm}_{lpk}(s,m_1,m_2)=\int_{(m_1+m_2)^2}^{\infty}\frac{ds'}{\pi}\,G^n_{lp}(s',m_1,m_2)\times\frac{\Phi_p(s',m_1,m_2)}{s'-s}\,G^m_{pk}(s',m_1,m_2). \tag{23}$$

We emphasize that the function B^{nm}_{ljk}, which characterizes the single-loop quark–antiquark diagrams, depends on the running quark and antiquark masses. Equation (22) can be readily rewritten in matrix form and solved explicitly.

2. In the next step, we replace the quark singularities on the first physical sheet by hadronic singularities, integrating in each quark–antiquark loop over the quark and antiquark mass distributions:

$$B(s)=\int_{\mu^2}^{\infty}dm_1^2\rho(m_1)\int_{\mu^2}^{\infty}dm_2^2\rho(m_2)B(s,m_1,m_2)\Theta(m_1+m_2-M_{\text{thr}}). \tag{24}$$

Here the Θ function is a cutoff that must be made when the quark mass is below the threshold of the first energetically allowed hadronic channel with mass M_{thr}. If all the lowest two-meson states are taken into account explicitly in the calculation, then M_{thr} is taken equal to the threshold of the lowest three-meson state that is allowed in the given partial-wave amplitude. For example, for the calculation of the amplitude with quantum numbers $J^{PC}=1^{--}$, the imaginary part of the quark–antiquark single-loop diagram must begin at the three-pion threshold for isospin 0 and at the $\pi\eta\pi$ threshold for isospin 1.

We consider the structure of the kernels $N_{ik}(s,s')$ that are used to calculate the amplitudes in our model. The initial quark–antiquark interaction was chosen in the form of the effective Lagrangian (2), (3) used to calculate the meson[15] and baryon[16] spectra in the framework of the bootstrap model. The kernel of the partial-wave amplitude (Fig. 8c) can be calculated by projecting this interaction into the s channel. After this, the expression must be decomposed into a sum of products of vertex functions $G(s)$ containing only left-hand singularities (such a decomposition is made in Appendix B). To eliminate the divergence in the quark–antiquark diagram, the integral (23) is regularized by the introduction of a cutoff function in the form (4).

The vertex of virtual transition of the S-wave mesons into a quark–antiquark pair is chosen in the form

$$\left(\bar q\,\frac{\tau}{2}[\gamma_5\boldsymbol{\pi}g_\pi+\gamma_\mu\boldsymbol{\rho}_\mu g_\rho]q\right)+\left(\bar q\,\frac{I}{2}[\gamma_5(\eta g_\eta\cos\alpha+\eta' g_{\eta'}\sin\alpha)+\gamma_\mu\omega_\mu g_\omega]q\right)+(\bar s[\gamma_5(-\eta g_\eta\sin\alpha+\eta' g_{\eta'}\cos\alpha+\gamma_\mu\Phi_\mu g_\Phi]s)+(\bar q_i[\gamma_5 K_i g_K+\gamma_\mu K^*_{i\mu}g_{K*}]s)+(\bar s[\gamma_5\bar K_i g_K+\gamma_\mu\bar K^*_{i\mu}g_{K*}]g_i), \tag{25}$$

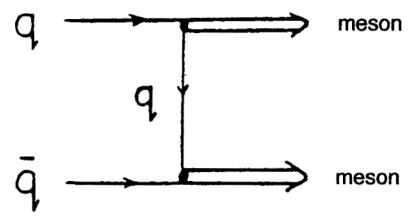

FIG. 9. The diagram describing the $q\bar q\to MM$ transition.

where α is the mixing angle of the pseudoscalar mesons, whereas the vectors mesons ω and Φ are taken as pure states of the nonstrange and strange quarks. For simplicity, $SU(3)$-symmetric coefficients are chosen:

$$g_\pi=g_K=g_\eta=g_{\eta'}\equiv g_1,\qquad g_\rho=g_\omega=g_\Phi=g_{K*}\equiv g_2. \tag{26}$$

The transition of the quark–antiquark pair into two mesons is described by the diagram shown in Fig. 9. The amplitude of this diagram is

$$A=(\bar\psi_2 Q^C\mathscr{G}(k)Q^B\psi_1)\varphi_3^{*B}\varphi_4^C F_1(k^2)F_2(k^2), \tag{27}$$

where k is the momentum of the exchanged quark, $\mathscr{G}(k)$ is its propagator, and $F_i(k^2)$ are the meson form factors. The operators Q^C and Q^B describe the meson $\to q\bar q$ transition and are determined by Eq. (25).

The propagator of the exchanged quark can differ quite strongly from the propagator of the constituent quark. In the considered approach, we have not attempted to solve the problem of the actual form of this propagator, and we have also not attempted to determine the structure of the form factors; rather, we have parametrized in very simple form the partial-wave interactions [the results of projecting the interaction (27) into the different partial waves] and determined the parameters on the basis of the best description of the experimental data. The total interaction (27) can be expressed as the sum of the partial-wave interactions in the following form:

$$A=\sum(\bar\psi_2 Q^C_j\psi_1)(\varphi_3^* O^C_j\varphi_4)N^j_{12}(s)=\sum(\bar\psi_2 Q^C_j\psi_1)(\varphi_3^* O^C_j\varphi_4)f_j(s)\beta_f. \tag{28}$$

Here the functions $f_j(s)$ determine the partial-wave interactions, and the coefficients β_f are the isotopic coefficients of the projection of the diagram of Fig. 9 into the different quark–antiquark and meson–meson isotopic channels. The list of these coefficients is given in Appendix C. The functions f_j have only left-hand singularities of the total amplitude (including rescattering of the particles), and we have parametrized these functions in the form of a product of two vertex functions that also have only left-hand singularities:

$$f_j(s)=4\pi^2 C_j G_{q\bar q}(s)G_{\mu\mu}(s), \tag{29}$$

where C_j are parameters that depend on the quantum numbers J^P. The functions $G(s)$ were chosen in a form that ensures convergence of the single-loop meson diagrams:

TABLE III. Masses and partial widths of $J^{PC}=1^{+-}$ mesons. The resonance masses are defined in the same way as in Table II. All quantities are given in mega-electron-volts.

Calculated quantity	m_q=390 Δ=0	m_q=625 Δ=0	m_q=625 Δ=100	m_q=625 Δ=200	Experiment
$m(h_1)$	-	1190	1190	1188	1170±20
Γ_{tot}	-	102	146	192	360±40
$\Gamma_{\rho\pi}$	-	100%	100%	100%	seen
$m(b_1)$	-	1240	1245	1242	1233±10
Γ_{tot}	-	30	44	98	150±10
$\Gamma_{\omega\pi}$	-	100%	100%	100%	dominant
$m(K_1)$	-	1245	1235	1190	1270±10
Γ_{tot}	-	86	100	90	90±20
$\Gamma_{K^*\pi}$	-	95%	100%	100%	20%
$\Gamma_{K\rho}$	-	5%	-	-	40%
$\Gamma_{K_0\pi}$	-	-	-	-	30%
$m(h_1)$	-	1610	1610	1608	-
Γ_{tot}	-	130	160	190	-
$\Gamma_{q\bar{q}}$	-	23%	23%	23%	
$\Gamma_{s\bar{s}}$	-	14%	13%	12%	
$\Gamma_{K^*\pi}$	-	35%	36%	37%	
$\Gamma_{\rho\pi}$	-	14%	14%	14%	
$\Gamma_{\Phi\eta}$	-	14%	14%	14%	

$$G_{q\bar{q}}=\lambda_q\sqrt{\frac{(m_1+m_2)^2-s_q}{s-s_q}},$$

$$G_{\mu\mu}=\sqrt{\frac{(\mu_1+\mu_2)^2-s_q'}{s-s_q'}}\left(1+\frac{s-(\mu_1+\mu_2)^2}{s}\alpha\right), \tag{30}$$

where

$$s_q=(m_1+m_2)^2-a_q,$$

$$s_q'=(\mu_1+\mu_2)^2-a_q. \tag{31}$$

The coefficient λ_q serves to distinguish the process of exchange of a nonstrange quark from the exchange of a strange one. This coefficient is equal to unity for exchange of a nonstrange quark ($\lambda_u=\lambda_d=1$), and in the case of exchange of a strange quark it is used as a fitting parameter. Similarly, the coefficient a_q is taken equal to 1 GeV^2 for exchange of a nonstrange quark and equal to $a_s=a_q m_s^2/m_q^2$ for exchange of a strange one. The parameter α is chosen to be the same for all channels.

6. THE PARAMETERS AND THEIR INFLUENCE ON THE RESULTS OF THE CALCULATIONS

We discuss the results of the calculation of the meson spectrum that are obtained by means of the model presented in Sec. 5, in which, in addition to the quark–antiquark channel, explicit allowance is made for the scattering channels of the pseudoscalar and vector mesons (S-wave states of a quark–antiquark pair). At the same time, we have advanced into the region of large values of the mean quark mass: In the distribution function $\rho(m)$, the mass m_0 is taken to be 625 MeV for a nonstrange quark and 800 MeV for a strange quark. The results of the calculation of the spectrum of S- and P-wave $q\bar{q}$ bound states for different widths of the mass distribution function are given in Tables I–V. The values of the parameters used in these calculations are given in Table VI.

TABLE IV. Masses and partial widths of $J^{PC}=1^{++}$ mesons. The resonance masses are defined in the same way as in Table II. All quantities are given in mega-electron-volts.

Calculated quantity	m_q=390 Δ=0	m_q=625 Δ=0	m_q=625 Δ=100	m_q=625 Δ=200	Experiment
$m(f_1)$	-	1283	1286	1287	1282±5
Γ_{tot}	-	38	46	70	24±3
$\Gamma_{q\bar{q}}$	-	100%	100%	100%	-
$m(a_1)$	-	1268	1274	1270	1260±30
Γ_{tot}	-	50	84	120	350–500
$\Gamma_{\rho\pi}$	-	62%	60%	71%	dominant
$\Gamma_{q\bar{q}}$	-	38%	40%	29%	-
$m(K_1)$	-	1350	1310	1260	1400±10
Γ_{tot}	-	128	100	92	175±20
$\Gamma_{K^*\pi}$	-	57%	85%	95%	94%
$\Gamma_{K\rho}$	-	33%	10%	5%	3%
$\Gamma_{K\omega}$	-	10%	5%	-	1%

The data on the meson scattering amplitudes are represented in terms of the phase shifts and inelasticities in the meson channels. In the case of the presence of the three scattering channels, the S matrix can be written in the form

$$S=\begin{pmatrix} \eta_{11}e^{2i\varphi_{11}} & \eta_{12}e^{2i\varphi_{12}} & \eta_{13}e^{2i\varphi_{13}} \\ \eta_{21}e^{2i\varphi_{21}} & \eta_{22}e^{2i\varphi_{22}} & \eta_{23}e^{2i\varphi_{23}} \\ \eta_{31}e^{2i\varphi_{31}} & \eta_{32}e^{2i\varphi_{32}} & \eta_{33}e^{2i\varphi_{33}} \end{pmatrix}. \tag{32}$$

Using the unitarity condition $SS^+=1$, we can readily show that only six elements of the S matrix are independent. As these independent elements, it is convenient to choose three phase shifts in the diagonal transitions, φ_{ii}, and three inelasticities: η_{ii}. In the case of a two-channel interaction, there are only three independent variables: two phase shifts φ_{11}, φ_{22} and the inelasticity parameter $\eta=\eta_{11}=\eta_{22}$.

TABLE V. Masses and partial widths of $J^{PC}=2^{++}$ mesons. The resonance masses are defined in the same way as in Table II. All quantities are given in mega-electron-volts.

Calculated quantity	m_q=390 Δ=0	m_q=625 Δ=0	m_q=625 Δ=100	m_q=625 Δ=200	Experiment
$m(f_2)$	-	1260	1263	1260	1275±5
Γ_{tot}	-	180	194	216	185±20
$\Gamma_{\pi\pi}$	-	80%	71%	65%	85%
$\Gamma_{K\bar{K}}$	-	15%	14%	10%	5%
$\Gamma_{q\bar{q}}$	-	5%	17%	25%	10%
$m(a_2)$	-	1280	1282	1281	1318±1
Γ_{tot}	-	44	44	42	110±5
$\Gamma_{K\bar{K}}$	-	29%	21%	15%	6%
$\Gamma_{\pi\eta}$	-	11%	7%	5%	14%
$\Gamma_{\rho\pi}$	-	3%	2%	2%	70%
$\Gamma_{q\bar{q}}$	-	57%	70%	78%	10%
$m(K_2)$	-	1440	1445	1450	1425±1
Γ_{tot}	-	60	60	96	98±3
$\Gamma_{K\pi}$	-	64%	56%	44%	50%
$\Gamma_{K\eta}$	-	5%	5%	4%	-
$\Gamma_{K^*\pi}$	-	2%	2%	2%	25%
Γ_{qs}	-	29%	37%	50%	25%

TABLE VI. Parameters of the model. The quark masses and widths of the quark mass distributions are given in mega-electron-volts.

Calculated quantity	$m_q=625$ $m_s=800$ $\Delta=0$	$m_q=625$ $m_s=800$ $\Delta=100$	$m_q=625$ $m_s=800$ $\Delta=200$
g_V	13.108	13.244	13.842
g_I	−2.3110	−2.3054	−2.4574
g_S	−1.2360	−1.2430	−1.2760
Λ	4.6821	4.6768	4.6846
$C(0^-)=C(1^-)$	7.85	7.98	8.38
$C(0^{++})$	14.34	14.46	15.01
$C(1^{+-})$	29.89	31.41	36.03
$C(1^{++})$	25.58	28.37	32.54
$C_S(2^{++})$	25.20	44.33	64.44
$C_D(2^{++})$	55.44	48.76	38.66
α	0.75	0.75	0.75
λ_s	1.3	1.3	1.3
g_1/g_2	2	2	2

The inelasticity parameters and the phase shifts for the scattering of the pseudoscalar and vector mesons in the states $J^{PC}=1^{--}, 0^{++}, 1^{++}, 1^{+-}, 2^{++}$ up to energy $\sqrt{s}=1.250$ GeV are given in Figs. 10–20.

We discuss the parameters of the model. For the description of the spectrum of low-lying mesons ($J^P=0^-$, 1^-), we use five parameters: The coupling constant g_V for exchange of the effective gluon, the coupling constants of the instanton interaction in the nonstrange channel, g_I, and in the strange channel, g_S, the cutoff parameter Λ, and the coupling constant for the $q\bar{q}\to MM$ transition, which is taken to be the same for both the $J^P=0^-$ and the 1^- channels: $C(0^-)=C(1^-)$. These parameters are found from the fitting of the masses of the π, K, η', ρ mesons and the width of the ρ meson.

To describe the meson–meson scattering in the $J^{PC}=0^{++}$ channel, three further parameters are used: the coupling constant $C(0^{++})$ for transition of a quark–antiquark pair into mesons and the parameters α and λ_s of the two-meson vertex function (30). Note that the last two parameters are common to all the scattering channels $J^{PC}=0^{++}$, 1^{+-}, 1^{++}, 2^{++}. The parameter α is most important for describing the phase shift in pion S-wave scattering at low energies. If this parameter is set equal to zero, it is possible to reproduce the meson spectrum without significant changes, but in S-wave pion–pion scattering a peak appears near the two-pion threshold. In the other channels, practically nothing like this occurs, since in them the meson–meson amplitude is either in the P or in the D wave and, therefore, is suppressed at the threshold, or the $q\bar{q}\to MM$ coupling constant is insufficiently strong to give rise to such an effect. The parameter

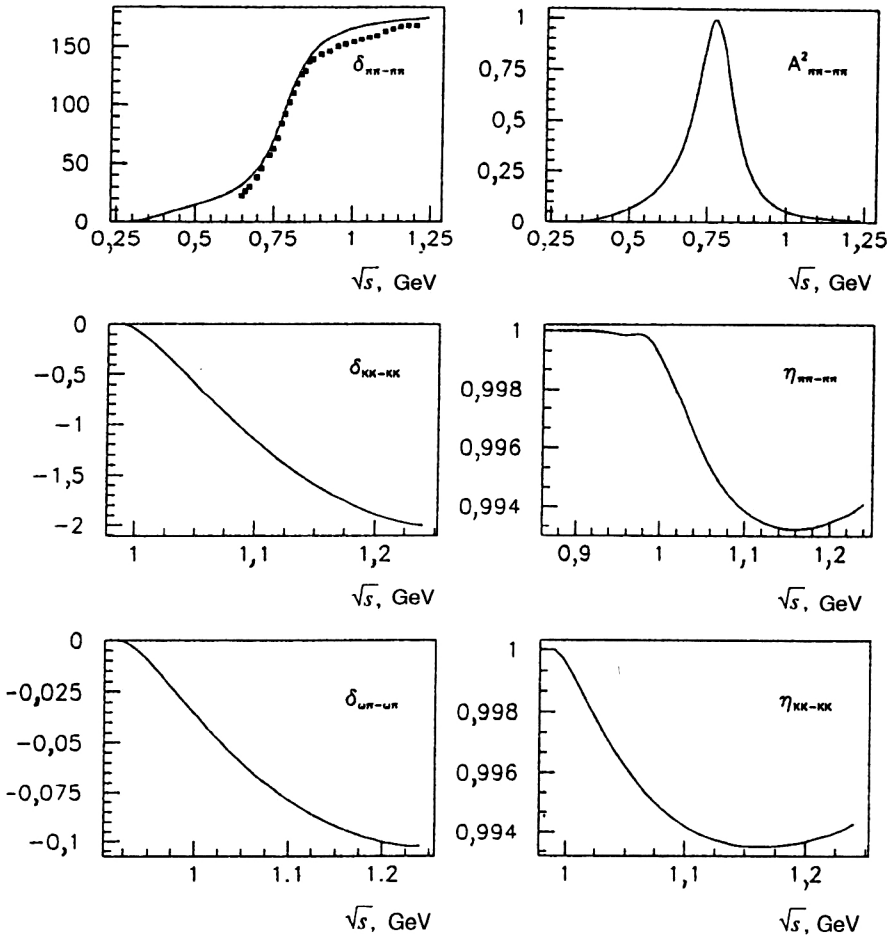

FIG. 10. Square of the $\pi\pi$ scattering amplitude, phase shifts, and inelasticities in the $I^GJ^{PC}=1^+1^{--}$ channel. The experimental data on the $\pi\pi$ phase shift are taken from Ref. 49.

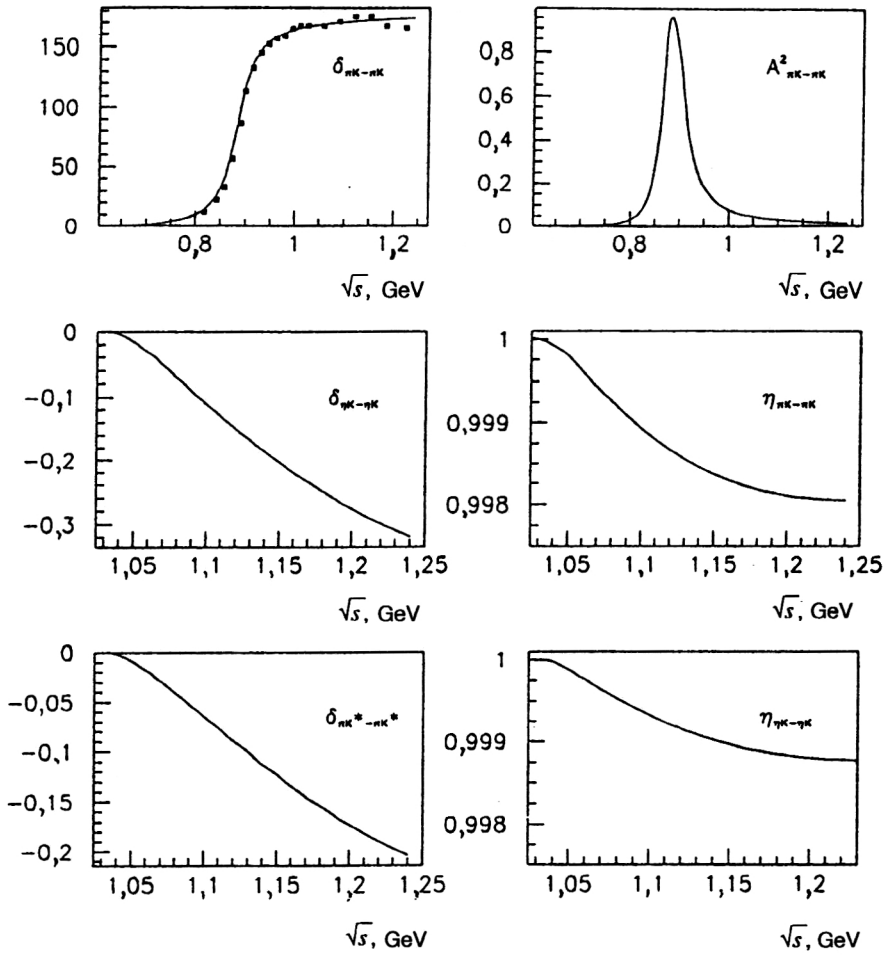

FIG. 11. Square of the πK scattering amplitude, phase shifts, and inelasticities in the $IJ^P=1/2\ 1^-$ channel. The experimental data on the πK phase shift are taken from Refs. 50 and 51.

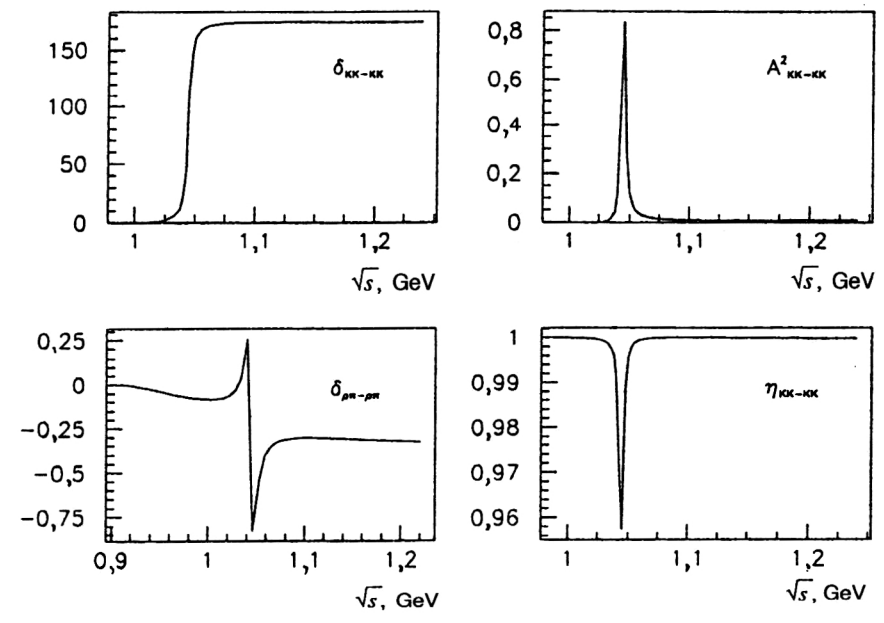

FIG. 12. Square of the $K\bar{K}$ scattering amplitude, phase shifts, and inelasticities in the $I^GJ^{PC}=0^-1^{--}$ channel.

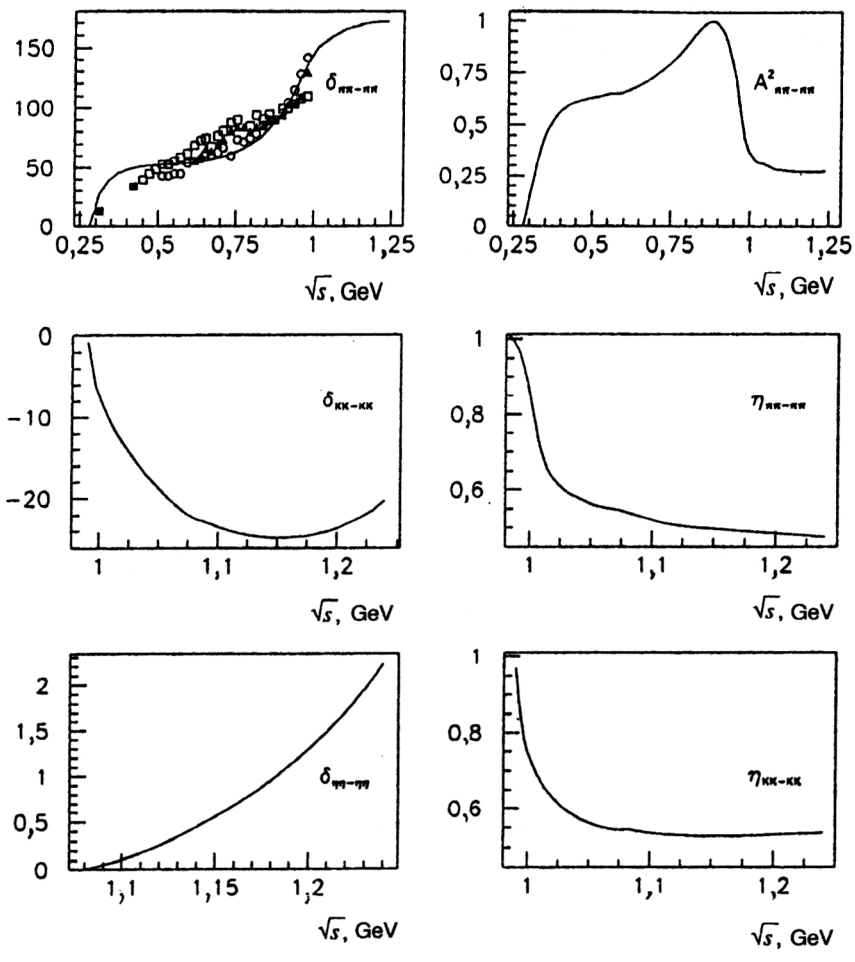

FIG. 13. Square of the $\pi\pi$ scattering amplitude, phase shifts, and inelasticities in the $I^G J^{PC}=0^+0^{++}$ channel. The experimental data on the $\pi\pi$ phase shift are taken from Refs. 49, 52, and 53.

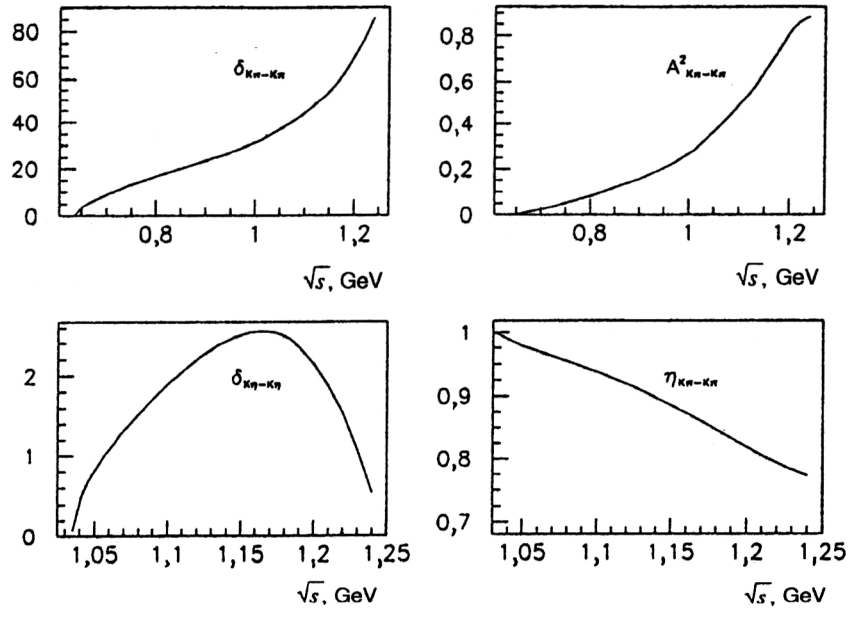

FIG. 14. Square of the πK scattering amplitude, phase shifts, and inelasticities in the $IJ^P=1/2\ 0^+$ channel.

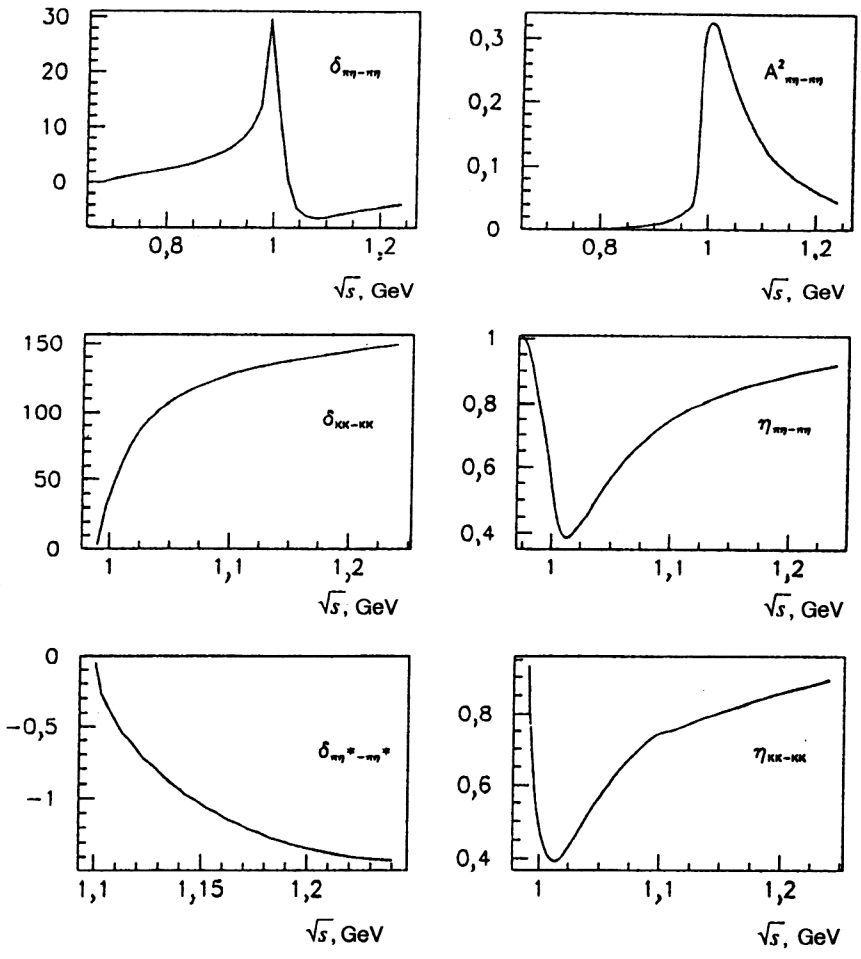

FIG. 15. Square of the $\pi\eta$ scattering amplitude, phase shifts, and inelasticities in the $I^GJ^{PC}=1^-0^{++}$ channel.

α cannot be taken to be large, since in this case it begins to influence the region of energies around 1 GeV, seriously affecting the spectrum of the 0^+ mesons. We note that the enhancement of the pion–pion S wave at low energies is also a consequence of the choice of the very simple parametrization of the $q\bar{q}\to MM$ transition.

As recent investigations have shown,[35,36,46] the pion–pion scattering amplitude in the S-wave channel near the K-meson threshold has a double pole structure: a comparatively narrow pole, which is called the f_0 resonance with mass $M=975$ and width 70–100 MeV, and a broad resonance with a mass of about 1 GeV. In our model, we have not obtained a narrow pole, but we have obtained a broad one with mass $M=900-i320$ MeV. This pole recalls the old ε (or σ) resonance that plays an important role in nucleon–nucleon interactions. The fact that the narrow f_0 resonance has not appeared in our model as a $q\bar{q}$ state leaves the possibility of explaining this resonance as some exotic state (see, for example, the discussion in Ref. 33 and the references given there). Our results in the scalar and isovector sectors agree fairly well with Flatté's parametrization of the a_0 resonance.[48] Although the determinant of the $\pi\eta$ scattering amplitude becomes purely imaginary at $M_{\pi\eta}=1.020$ GeV, the square of the amplitude has a maximum at the $K\bar{K}$ threshold, and if this amplitude is fitted by a Breit–Wigner pole, the resulting mass and width are very close to the values given by the Particle Data Group.[35]

In the $J^{PC}=1^{+-}$ and $J^{PC}=1^{++}$ channels, two new parameters are introduced: the coupling constants $C(1^{++})$ and $C(1^{+-})$ of the $q\bar{q}\to MM$ transition. In the strange sector, these channels are mixed, and the properties of the K_1 mesons are calculated with allowance for this mixing.

In the $J^{PC}=2^{++}$ channel, two additional parameters are also introduced: the coupling constant of the $q\bar{q}$ with the mesons in the S wave, $C_S(2^{++})$, and with the mesons in the D wave, $C_D(2^{++})$. The second parameter is fixed in such a way as to give the correct width of the $f_2(I^GJ^{PC}=0^+2^{++})$ meson, and the first is chosen in order to give the best description of the meson spectrum in this channel. We mention that the model did not describe the resonance with mass $M=1525$ MeV in the isoscalar channel, which is usually assumed to be a bound state of strange quarks. It appears that this meson is formed as a result of strong mixing of all the channels and, therefore, must appear in the next step in the model when allowance is made for the channels with scattering of P-wave mesons.

Besides the parameters listed above and used in the model, two further parameters, which are common to all channels, are used: the mean mass m_q of a nonstrange quark and the ratio of the coupling constants for transition of pseu-

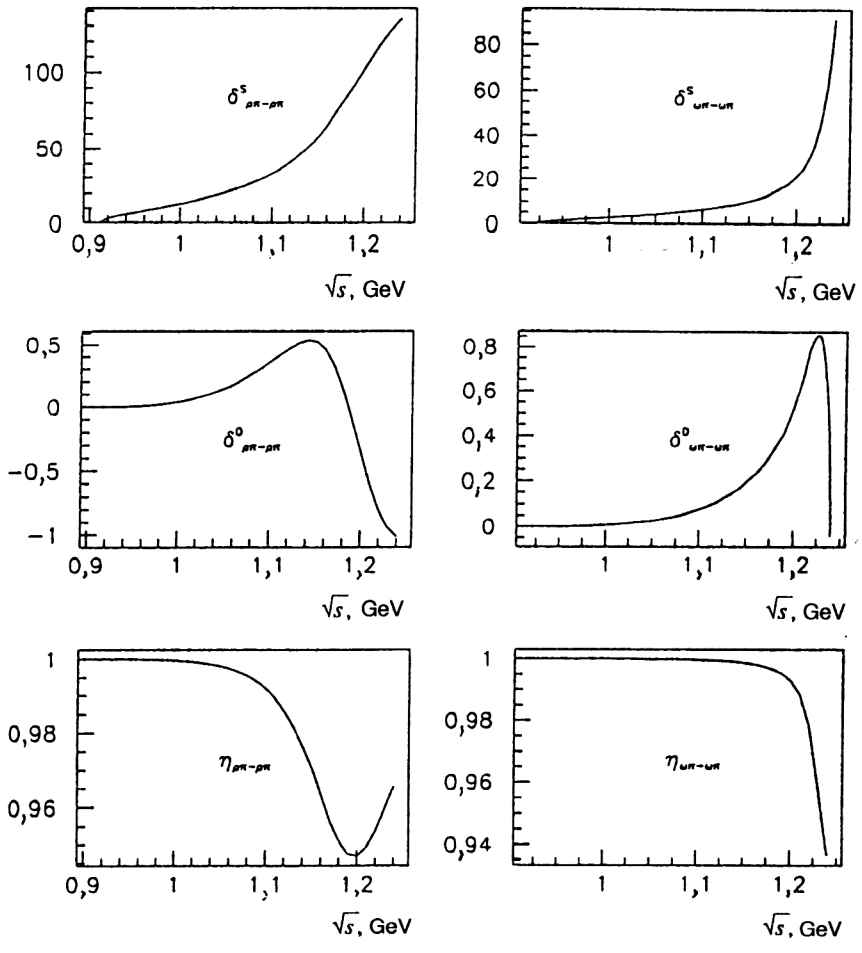

FIG. 16. The S- and D-wave phase shifts and mixing parameters in the $I^GJ^{PC}=0^-1^{+-}$ channel ($\rho\pi$ scattering) and in the $I^GJ^{PC}=1^+1^{+-}$ channel ($\omega\pi$ scattering).

doscalar and vector mesons into a quark–antiquark pair: g_1/g_2 [see Eq. (26)].

The spectrum of the $J^P=0^-$, 1^-, 0^+ mesons is practically independent of the nonstrange quark mass when this mass is varied in the range 500–800 MeV. Our mass 625 MeV of the nonstrange quark gives the best description of the meson spectrum in the $J^{PC}=1^{++}$, 2^{+-}, 2^{++} channels.

The mass of the strange quark was shifted while keeping fixed the ratio of the masses of the strange and nonstrange quarks obtained in Ref. 15:

$$\frac{m_q}{m_s}=\frac{m_q^{\text{old}}}{m_s^{\text{old}}}, \tag{33}$$

where $m_q^{\text{old}}=390$ MeV and $m_s^{\text{old}}=500$ MeV.

The parameter g_1/g_2 is fairly strongly correlated with the parameter λ_s and can be used to obtain a reasonable splitting of the ω and Φ mesons.

7. CONCLUSIONS

Low-energy soft processes can be successfully described by the QCD-motivated quark model. Although the basic theory, QCD, does not make it possible to calculate directly the majority of characteristics of the quark model, nevertheless the success of this model in describing physical processes indicates that the main features of the physics at distances around 0.3–1.0 F are taken into account correctly.

One of the aims in the construction of the model was to investigate the possibility of taking into account confinement forces induced by $q\bar{q}\to$meson+meson transitions. For this, we started with a bootstrap model, in which, in the framework of a purely quark description, we obtained the spectrum of the low-lying mesons and in which of the corresponding hadronic degrees of freedom can be included relatively simply. In the first stage, the stage of the bootstrap calculations, the constituent quark had a mass 350–400 MeV (the mass of the strange quark was 150–200 MeV greater), and the interaction was due to exchange of an effective gluon and to instanton-induced forces. Such a model gives a good description of the spectrum of $J^P=0^-$, 1^- mesons and gives a qualitatively correct description of the spectrum of $J^P=0^+$ mesons.

Mesonic degrees of freedom are included in the model by means of the amplitudes of $q+\bar{q}\to q+\bar{q}q+\bar{q}\to M+M$ transitions, which are intimately related to the confinement mechanism: The outgoing quarks create quark–antiquark pairs, which go over into mesons. In this second stage, we have included in the calculations only the scattering channels of the low-lying mesons, i.e., the states obtained in the framework of the bootstrap procedure. The $q\bar{q}\to M$

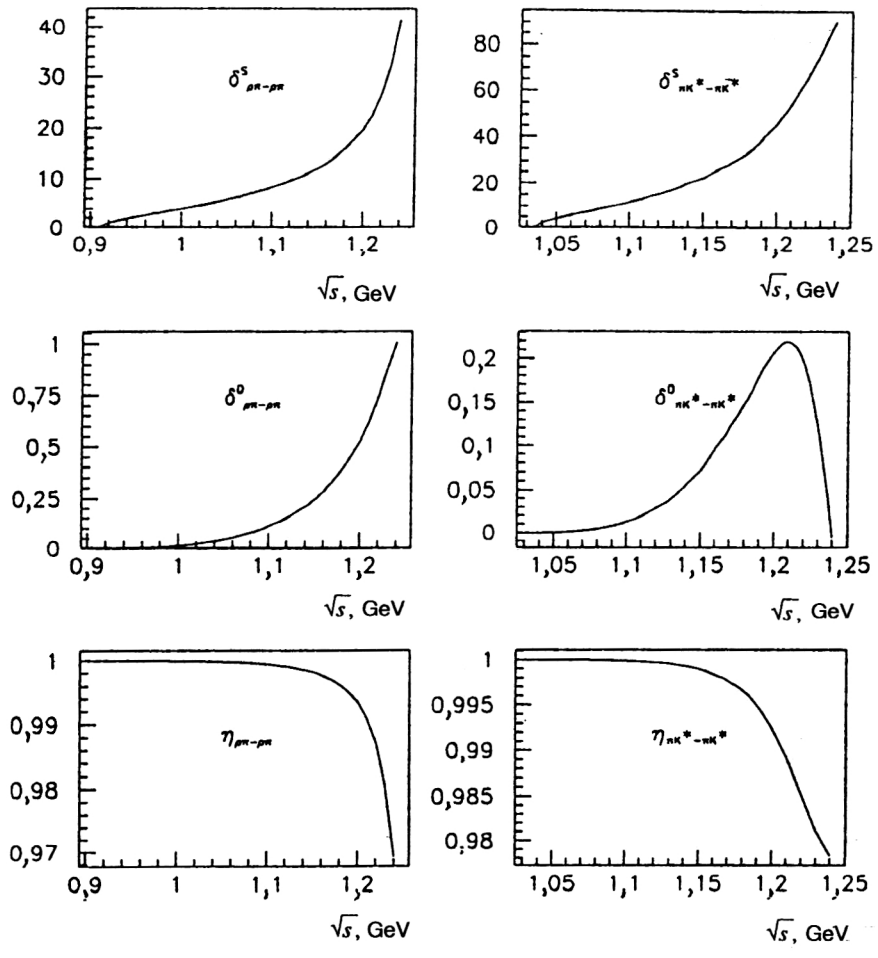

FIG. 17. The S- and D-wave phase shifts and mixing parameters in the $I^G J^{PC}=1^-1^{++}$ channel ($\rho\pi$ scattering) and in the $IJ^P=1/2\ 1^+$ (πK^* scattering).

$+M\to q\bar{q}$ transitions lead to an effective $q\bar{q}$ interaction, which plays the role of a confinement barrier responsible for the forces in the region of 1 F and, therefore, for the formation of the mesonic states with mass greater than 1 GeV.

In the framework of this model with allowance for $q+\bar{q}\to M+M$ transitions we obtained the following results:

1. We have calculated the masses and widths of the 0^- and 1^- mesons, which are in good agreement with the experimental data.

2. We have calculated the spectroscopic properties of the highly excited mesons with masses 1.0–1.5 GeV (P-wave $q\bar{q}$ states): They are in qualitative agreement with the experimental data.

3. We have obtained the amplitudes of meson–meson scattering, which also agree satisfactorily with the experiment.

The explicit inclusion in the model of the mesonic degrees of freedom leads to the following changes in the quark dynamics:

1. A significant fraction of the splitting and mixing of the low-lying mesonic states is determined by the $\bar{q}q\to MM$ interaction. The contribution of the instanton-induced forces is accordingly weakened.

2. The quark mass is increased by about 200 MeV for both the nonstrange and the strange quarks.

This is in fact a direct indication of the mechanism of quark–hadron duality: The quark properties are intimately related to a definite set of hadronic states. If the low-lying mesons are taken into account in the model explicitly and, therefore, eliminated from this set, then for the quarks a new higher scale of energies and masses is established, and this leads to an effectively higher mass of a new "constituent quark."

We thank the theoreticians at the Institute of Nuclear Physics at the University of Bonn, and especially B. C. Metsch, H. R. Petry, and V. N. Gribov for numerous fruitful discussions.

8. APPENDIX A

We consider the structure of the operators of the partial waves in two-particle scattering. These operators can be constructed by means of the orthogonality condition given in Eq. (16). Another condition used in the construction of the operators is the condition that these operators in the center-of-mass system be identical to the ordinary nonrelativistic operators. On the basis of this, we obtain the following spectrum of operators for the S- and P-wave states of two fermions:

$i\gamma_5$ for $^1S_0$ $J^{PC}=0^{-+}$

$i\Gamma_\mu$ for $^3S_1$ $J^{PC}=1^{--}$

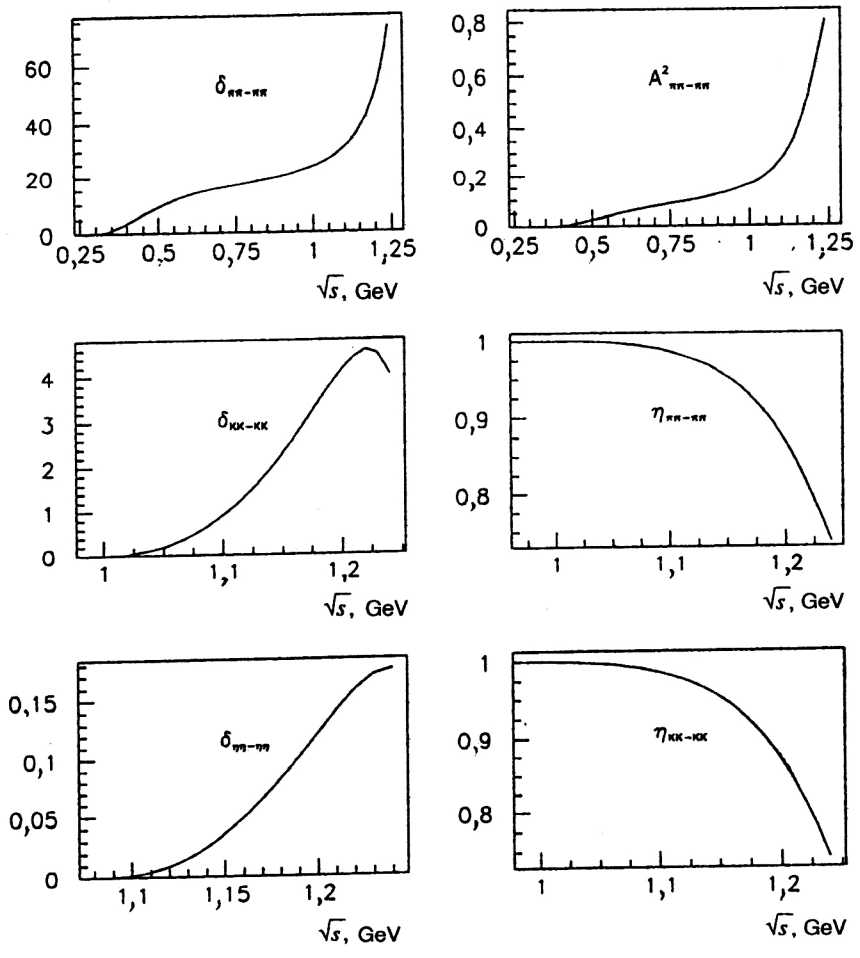

FIG. 18. Square of the $\pi\pi$ scattering amplitude, phase shifts, and inelasticities in the $I^GJ^{PC}=0^+2^{++}$ channel.

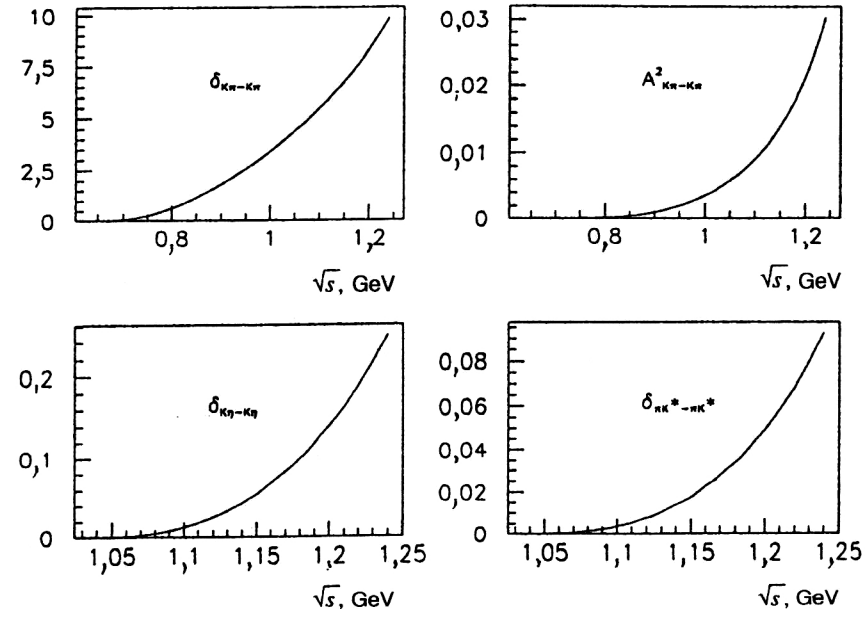

FIG. 19. Square of the πK scattering amplitude, phase shifts, and inelasticities in the $IJ^P=1/2\ 2^+$ channel.

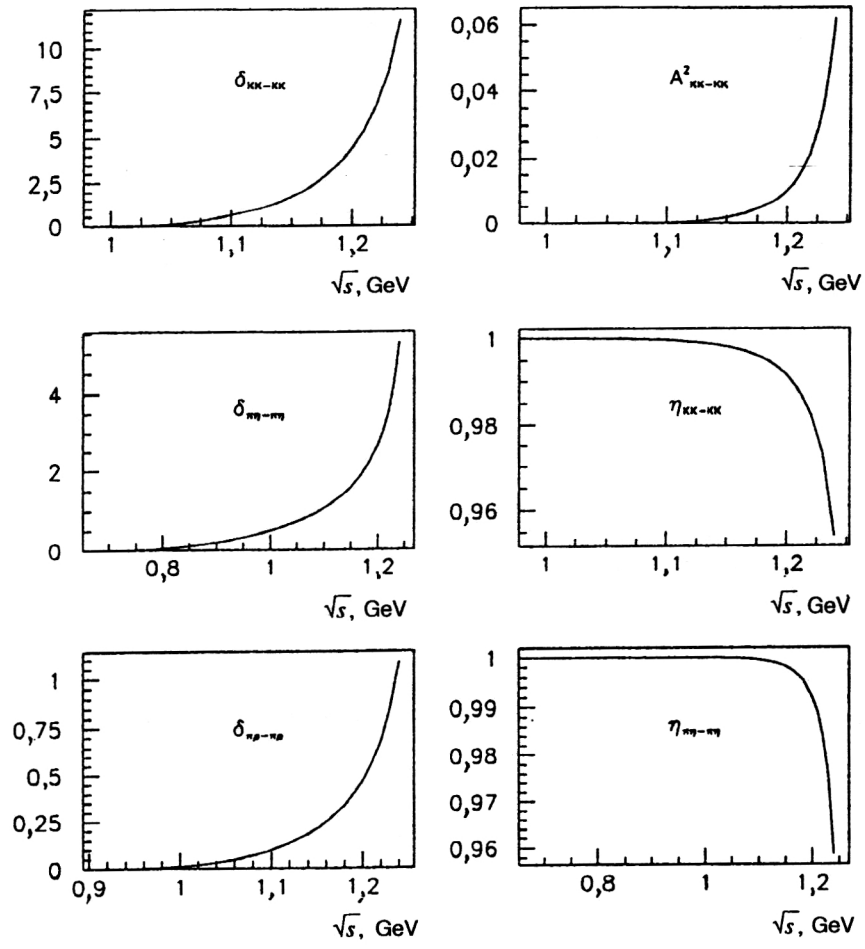

FIG. 20. Square of the KK scattering amplitude, phase shifts, and inelasticities in the $I^G J^{PC}=1^-2^{++}$ channel.

$$1 \quad \text{for } {}^1P_0 \quad J^{PC}=0^{++}$$

$$\frac{\sqrt{3}}{\sqrt{s}}\gamma_5 k_\mu^\perp \quad \text{for } {}^1P_1 \quad J^{PC}=1^{+-}$$

$$\frac{\sqrt{3}}{\sqrt{2}s}\varepsilon_{\mu ijk}k_i^\perp P_j\gamma_k \quad \text{for } {}^3P_1 \quad J^{PC}=1^{++}$$

$$\frac{\sqrt{3}}{2\sqrt{s}}\Gamma_i k_j^\perp O_{\mu\nu}^{ij} \quad \text{for } {}^3P_2 \quad J^{PC}=2^{++}, \tag{34}$$

where

$$k_\mu^\perp=\frac{1}{2}\left[(p_1-p_2)_\mu-\frac{m_1^2-m_2^2}{P^2}P_\mu\right],$$

$$\gamma_\mu^\perp=\gamma_\mu-\frac{P_\mu\hat{P}}{P^2},$$

$$\Gamma_\mu=\gamma_\mu^\perp-\frac{2k_\mu^\perp}{m_1+m_2+\sqrt{P^2}},$$

$$g_{\mu\nu}^\perp=g_{\mu\nu}-\frac{P_\mu P_\nu}{P^2},$$

$$O_{ij}^{\mu\nu}=\frac{1}{2}\left(g_{\mu i}^\perp g_{\nu j}^\perp+g_{\mu j}^\perp g_{\nu i}^\perp-\frac{2}{3}g_{\mu\nu}^\perp g_{ij}^\perp\right). \tag{35}$$

The operator δ_{BC} introduced in Eq. (16) is a projection operator and is equal to unity for states with total angular momentum $J=0$ and to $g_{\mu\nu}^\perp$ for states with $J=1$. The partial-wave operators are normalized by the phase-space functions $\Phi(k)$, which are

$$\Phi(s)=2(s-(m_1-m_2)^2)\Phi_S(s) \quad \text{for } J^P=0^-,1^-$$

$$\Phi(s)=2(s-(m_1+m_2)^2)\Phi_S(s) \quad \text{for } J^P=0^+$$

$$\Phi(s)=2(s-(m_1-m_2)^2)\frac{\mathbf{k}^2}{s}\Phi_S(s) \quad \text{for } J^P=1^+,2^+, \tag{36}$$

where

$$\Phi_S(s)=\frac{|\mathbf{k}|}{8\pi\sqrt{s}},$$

$$\mathbf{k}^2=-k^{\perp 2}=\frac{(s-(m_1+m_2)^2)(s-(m_1-m_2)^2)}{4s}. \tag{37}$$

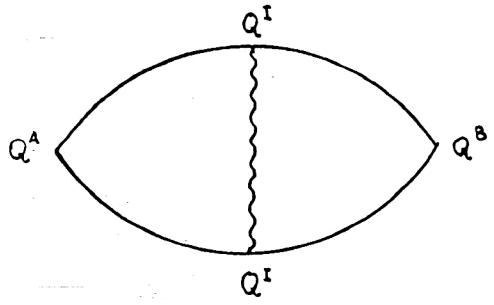

FIG. 21. Two-loop diagram for calculating the projection of the t-channel interaction determined by the operator Q_I onto the s-channel partial wave determined by the operator Q_j^B.

The partial-wave operators for two-boson scattering must satisfy the orthogonality condition given in (17)–(19). This leads to the following spectrum of scattering operators of two pseudoscalar (or scalar) bosons:

$$1 \quad \text{for } {}^1S_0 \quad J^{PC}=0^+$$

$$\frac{i}{\sqrt{s}}k_\mu^\perp \quad \text{for } {}^1P_1 \quad J^{PC}=1^-$$

$$\frac{\sqrt{5}}{\sqrt{6}s}K_{\mu\nu} \quad \text{for } {}^1D_2 \quad J^{PC}=2^+, \tag{38}$$

where

$$K_{\mu\nu}=k_\mu^\perp k_\nu^\perp-\frac{1}{3}g_{\mu\nu}^\perp k^{\perp 2}, \tag{39}$$

and the vector $k_\mu^\perp$ and the operator $g_{\mu\nu}^\perp$ are defined in the same way as in the case of fermion scattering.

To construct the spectrum of scattering operators of the vector and pseudoscalar bosons, we introduce the operators

$$\Gamma^1_{\alpha\beta}=g^\perp_{\alpha\beta}-\frac{k^\perp_\alpha k^\perp_\beta}{k^{\perp 2}}\frac{(\sqrt{s}-M)(\sqrt{s}-\delta)}{s+M\delta},$$

$$\tilde{k}^\perp_{1\alpha}=k^\perp_\beta\Gamma^1_{\alpha\beta}, \tag{40}$$

where

$$M=\mu_1+\mu_2 \quad \delta=\mu_1-\mu_2. \tag{41}$$

In the center-of-mass system of the compound system, the operator $\Gamma^1_{\alpha\beta}$ carries the relativistic four-dimensional polarization vector of the boson into a nonrelativistic three-dimensional vector. By means of these operators, the spectrum of partial-wave scattering operators for the vector and pseudoscalar bosons can be written as follows:

$$\Gamma^1_{\mu\alpha} \quad \text{for } {}^3S_1 \quad J^P=1^+$$

$$\frac{i}{\sqrt{s}}\tilde{k}^\perp_{1\alpha} \quad \text{for } {}^3P_0 \quad J^P=0^-$$

$$\frac{\sqrt{3}}{\sqrt{2}s}\varepsilon_{\mu\alpha ij}k_i^\perp P_j \quad \text{for } {}^3P_1 \quad J^P=1^-$$

$$i\frac{\sqrt{3}}{2\sqrt{s}}\left[\Gamma^1_{\mu\alpha}k^\perp_\nu P_j+\Gamma^2_{\nu\alpha}k^\perp_\mu P_j-\frac{2}{3}g^\perp_{\mu\nu}\tilde{k}_{1\alpha}\right] \quad \text{for } {}^3P_2 \quad J^P=2^-$$

$$\frac{3}{\sqrt{2}s}\left[\tilde{k}^\perp_{1\alpha}k^\perp_\mu-\frac{1}{3}k^{\perp 2}\Gamma^1_{\mu\alpha}\right] \quad \text{for } {}^3D_1 \quad J^P=1^+$$

$$i\frac{\sqrt{5}}{2s\sqrt{s}}(k^\perp_\mu\varepsilon_{\nu\alpha ij}k^\perp_i P_j+k^\perp_\nu\varepsilon_{\mu\alpha ij}k^\perp_i P_j) \quad \text{for } {}^3D_2 \quad J^P=2^+, \tag{42}$$

where α is the polarization index of the vector meson. To construct the spectrum of the scattering operators of two vector bosons, we introduce the operator $\Gamma^2_{\alpha\beta}$, which is an analog of the operator $\Gamma^1_{\alpha\beta}$ but acts on the second particle:

$$\Gamma^2_{\alpha\beta}=g^\perp_{\alpha\beta}-\frac{k^\perp_\alpha k^\perp_\beta}{k^{\perp 2}}\frac{(\sqrt{s}-M)(\sqrt{s}+\delta)}{s-M\delta},$$

$$\tilde{k}^\perp_{2\alpha}=k^\perp_\beta\Gamma^2_{\alpha\beta}, \tag{43}$$

$$\Gamma^0_{\alpha\beta}=\Gamma^1_{\alpha\nu}\Gamma^2_{\nu\beta}. \tag{44}$$

The operators of the states of the system of two vector particles can be expressed in terms of the operators introduced above as follows:

$$\frac{1}{\sqrt{3}}\Gamma^0_{\alpha\beta} \quad \text{for } {}^1S_0 \quad J^P=0^+$$

$$\frac{i}{\sqrt{2}s}\varepsilon_{\mu\alpha'\beta' j}\Gamma^1_{\alpha'\alpha}\Gamma^2_{\beta'\beta}P_j \quad \text{for } {}^3S_1 \quad J^P=1^+$$

$$\frac{1}{2}\left[\Gamma^1_{\mu\alpha}\Gamma^2_{\nu\beta}+\Gamma^1_{\nu\alpha}\Gamma^2_{\mu\beta}-\frac{2}{3}g^\perp_{\mu\nu}\Gamma^0_{\alpha\beta}\right] \quad \text{for } {}^5S_2 \quad J^P=2^+$$

$$\frac{i}{\sqrt{3}s}k^\perp_\mu\Gamma^0_{\alpha\beta} \quad \text{for } {}^1P_1 \quad J^P=1^-$$

$$\frac{1}{\sqrt{3}s}\varepsilon_{\alpha\beta ij}k^\perp_i P_j \quad \text{for } {}^3P_0 \quad J^P=0^-$$

$$\frac{i}{2\sqrt{s}}[\Gamma^1_{\mu\alpha}\tilde{k}_{2\beta}-\Gamma^2_{\mu\beta}\tilde{k}_{1\alpha}] \quad \text{for } {}^3P_1 \quad J^P=1^-$$

$$\frac{\sqrt{3}}{4s}\left[k_\mu\varepsilon_{\nu\alpha'\beta' j}+k_\nu\varepsilon_{\mu\alpha'\beta' j}-\frac{2}{3}g^\perp_{\mu\nu}\varepsilon_{i\alpha'\beta' j}k_i\right]P_j\Gamma^1_{\alpha'\alpha}\Gamma^2_{\beta'\beta} \quad \text{for } {}^3P_2 \quad J^P=2^-$$

$$\frac{\sqrt{3}i}{\sqrt{20}s}\left[\Gamma^1_{\mu\alpha}\tilde{k}_{2\beta}+\Gamma^2_{\mu\beta}\tilde{k}^\perp_{1\alpha}-\frac{2}{3}k^\perp_\mu\Gamma^0_{\alpha\beta}\right] \quad \text{for } {}^5P_1 \quad J^P=1^-$$

$$\frac{1}{4s}[\Gamma^1_{\mu\alpha}\varepsilon_{\nu i\beta j}k^\perp_i P_j+\Gamma^2_{\mu\beta}\varepsilon_{\nu i\alpha j}k^\perp_i P_j+(\mu\rightarrow\nu)] \quad \text{for } {}^5P_2 \quad J^P=2^-$$

$$\frac{\sqrt{5}}{\sqrt{6}s}\Gamma^0_{\alpha\beta}\left(k^\perp_\mu k^\perp_\nu-\frac{k^{\perp 2}}{3}g^\perp_{\mu\nu}\right) \quad \text{for } {}^1D_2 \quad J^P=2^+$$

$$\frac{3i}{2s\sqrt{2s}}\left[k_\mu^\perp \varepsilon_{i\alpha\beta j}k_i P_j - \frac{k^{\perp 2}}{3}\varepsilon_{\mu\alpha'\beta' j}P_j\Gamma^1_{\alpha'\alpha}\Gamma^2_{\beta'\beta}\right] \quad \text{for } {}^3D_1 \ J^P=1^+$$

$$\frac{\sqrt{5}}{2s\sqrt{6}}[k_\nu^\perp(\Gamma^1_{\mu\alpha}\tilde{k}_{2\beta}-\Gamma^2_{\mu\beta}\tilde{k}_{1\alpha})+(\mu\to\nu)] \quad \text{for } {}^3D_2 \ J^P=2^+$$

$$\frac{\sqrt{3}}{\sqrt{2s}}\left[\tilde{k}_{1\alpha}\tilde{k}_{2\beta}-\frac{k^{\perp 2}}{3}\Gamma^0_{\alpha\beta}\right] \quad \text{for } {}^5D_0 \ J^P=0^+$$

$$\frac{\sqrt{3}i}{2s\sqrt{2s}}[\tilde{k}_{1\alpha}\varepsilon_{\mu i\beta j}k_i P_j+\tilde{k}_{2\beta}\varepsilon_{\mu i\alpha j}k_i P_j] \quad \text{for } {}^5D_1 \ J^P=1^+. \tag{45}$$

All the boson scattering operators given above are normalized in such a way that after summation over the different spin states they give the following phase spaces:

$$\Phi(s)=1 \quad \text{for } S\text{-wave state},$$

$$\Phi(s)=(s-M^2)(s-\delta^2)/4s^2 \quad \text{for } P\text{-wave state},$$

$$\Phi(s)=(s-M^2)^2(s-\delta^2)^2/16s^4 \quad \text{for } D\text{-wave state}. \tag{46}$$

9. APPENDIX B

We give the method for calculating the partial-wave vertex functions for the interaction determined by the Lagrangian (2). This Lagrangian determines both the s- and t-channel interactions of the $q\bar{q}$ pair. To calculate the N function, it is necessary to expand the t-channel interaction with respect to the s-channel partial-wave amplitudes. This procedure, which is essentially a Fierz transformation, can be carried out as the calculation of the product of the discontinuities of the amplitude in the two-loop diagram shown in Fig. 21. Since the operators Q_j^B of the partial-wave states introduced by means of the orthogonality condition (15)–(18) form a complete set, they automatically separate the required s-wave interaction from the t-channel interaction. As a result, we obtain an s-channel vertex function multiplied by the functions $\Phi_j(s)$ of the two-particle phase spaces.

The interaction block N_s^{ic}, where the index i corresponds to the isospin, c to the color, and s to the spin variables, is subjected to a Fierz transformation:

$$N_s^{ic}(s \text{ channel})=U^{ij}V^{cp}\hat{P}_{sl}N_l^{jp}(t \text{ channel}). \tag{47}$$

where

$$V=\frac{1}{3}\begin{bmatrix}1 & 8\\ 1 & -1\end{bmatrix}, \quad U=\frac{1}{2}\begin{bmatrix}1 & 3\\ 1 & -1\end{bmatrix}, \tag{48}$$

and the operator $\hat{P}$ is the operator of transformation of the spin variables. The matrix elements of this transformation are calculated as follows. Let the t-channel interaction be determined by means of the operators $Q^I(t)\otimes Q^I(t)$, where summation over the index I is understood; t indicates that these operators act in the t channel, and, in contrast to (15), we have for simplicity omitted the index labeling the total angular momentum. The projection of these operators onto the s-channel operators $Q^C(s)\otimes Q^C(s)$ is equal to (see Fig. 21)

$$P(Q^C(s)\otimes Q^C(s)\leftarrow Q^I(t)\otimes Q^I(t))=\frac{\langle \mathrm{Tr}[Q^B(m_1+\hat{k}_1)Q_I(m_1+\hat{k}_1')Q^A(m_2-\hat{k}_2')Q_I(m_2-\hat{k}_2)]\rangle}{\langle \mathrm{Tr}[Q^B(m_1+\hat{k}_1)Q^C(m_2-\hat{k}_2)]\mathrm{Tr}[Q^C(m_1+\hat{k}_1')Q^A(m_2-\hat{k}_2')]\rangle}, \tag{49}$$

where $\langle ... \rangle$ denotes integration with respect to the angle variables of the two-loop diagram in Fig. 21. We recall that in the calculation of the product of the discontinuities of the amplitude it is necessary to keep particles 1, 2 and 1′, 2′ on the mass shell. For the vector interaction $\gamma_\mu\otimes\gamma_\mu$ and the instanton interaction $(1+\gamma_5)\otimes(1+\gamma_5)$ considered in our case the decomposition with respect to s-channel partial waves gives the following result:

for $J^P=0^-$:

$$P(i\gamma_5\otimes i\gamma_5\leftarrow\gamma_\mu\otimes\gamma_\mu)=-1+(m_1+m_2)^2/(2s),$$

$$P(i\gamma_5\otimes i\gamma_5\leftarrow(1+\gamma_5)\otimes(1+\gamma_5))=1/2:$$

for $J^P=0^+$:

$$P(1\otimes 1\leftarrow\gamma_\mu\otimes\gamma_\mu)=-1+(m_1-m_2)^2/(2s);$$

$$P(1\otimes 1\leftarrow(1+\gamma_5)\otimes(1+\gamma_5))=-1/2;$$

for $J^P=1^-$:

$$P(i\Gamma_\mu\otimes i\Gamma_\mu\leftarrow\gamma_\mu\otimes\gamma_\mu)=-1/2-(s-(m_1+m_2)^2)/(6s))+(\sqrt{s}-m_1-m_2)^2/(9s),$$

$$P(i\Gamma_\mu\otimes i\Gamma_\mu\leftarrow(1+\gamma_5)\otimes(1+\gamma_5))=-s(-(m_1+m_2)^2)/(12s). \tag{50}$$

10. APPENDIX C

We give the isotopic coefficients $\beta(j_1,j_2,J|i_1,i_2,I)$ for the $q\bar{q}\to MM$ transition, where the indices j_1,j_2,J correspond, respectively, to the isospins of the quark and antiquark and the isospin of the $q\bar{q}$ composite system, and the indices i_1,i_2,I describe the isospins of the mesons and of their composite system:

$$\beta\left(\frac{1}{2},\frac{1}{2},1\middle|1,1,1\right)=-1, \quad \beta\left(\frac{1}{2},\frac{1}{2},1\middle|1,0,1\right)=\frac{1}{\sqrt{2}},$$

$$\beta\left(\frac{1}{2},\frac{1}{2},1\middle|\frac{1}{2},\frac{1}{2},1\right)=1,\quad \beta\left(\frac{1}{2},\frac{1}{2},0\middle|1,1,0\right)=\frac{\sqrt{3}}{\sqrt{2}},$$

$$\beta\left(\frac{1}{2},\frac{1}{2},0\middle|0,0,0\right)=\frac{1}{\sqrt{2}},\quad \beta\left(\frac{1}{2},\frac{1}{2},0\middle|\frac{1}{2},\frac{1}{2},0\right)=1,$$

$$\beta\left(\frac{1}{2},0,\frac{1}{2}\middle|1,\frac{1}{2},\frac{1}{2}\right)=\frac{\sqrt{3}}{\sqrt{2}},\quad \beta\left(\frac{1}{2},0,\frac{1}{2}\middle|\frac{1}{2},0,\frac{1}{2}\right)=1,$$

$$\beta\left(\frac{1}{2},0,\frac{1}{2}\middle|0,\frac{1}{2},\frac{1}{2}\right)=\frac{1}{\sqrt{2}},\quad \beta\left(0,0,0\middle|\frac{1}{2},\frac{1}{2},0\right)=\sqrt{2},$$

$$\beta(0,0,0|0,0,0)=1. \qquad (51)$$

[1] U. Häbel, R. Könning, H.-G. Reusch, M. Stingle, and S. Wigard, Z. Phys. A **336**, 423, **336**, 435 (1990).
[2] V. N. Gribov, Preprint LU TP-91-7 (1991).
[3] S. Weinberg, Phys. Rev. Lett. **65**, 1181 (1990).
[4] R. L. Jaffe, Phys. Lett. B **245**, 221 (1990).
[5] J. Ellis, Y. Frishman, and M. Karliner, Phys. Lett. B **272**, 333 (1991).
[6] H. Fritzsch, Preprint CERN-TH 7079/93 (1993).
[7] N. Isgur and G. Karl, Phys. Rev. D **18**, 4187 (1978); **19**, 2653 (1979); **20**, 1191 (1979).
[8] R. Startor and Fl. Stancu, Phys. Rev. D **31**, 128 (1985).
[9] S. Capstick and N. Isgur, Phys. Rev. D **34**, 2809 (1986).
[10] S. L. Adler and T. Piran, Rev. Mod. Phys. **56**, 1 (1984).
[11] M. Baker, J. S. Ball, and F. Zachariasen, Phys. Rev. D **31**, 2575 (1985); **34**, 3894 (1986).
[12] M. Creutz, *Quarks, Gluons and Lattices* (Cambridge University Press, Cambridge, 1983).
[13] C. Rebbi, *Lattice Gauge Theories and Monte Carlo Simulations* (World Scientific, Singapore, 1983).
[14] V. V. Anisovich, M. N. Kobrinsky, Yu. Nyiri, and Yu. M. Shabelski, *Quark Model and High Energy Collisions* (World Scientific, Singapore, 1985).
[15] V. V. Anisovich, S. M. Gerasyuta, and A. V. Sarantsev, Int. J. Mod. Phys. A **6**, 625 (1991).
[16] S. M. Gerasyuta and A. V. Sarantsev, Yad. Fiz. **52**, 1483 (1990) [Sov. J. Nucl. Phys. **52**, 937 (1990)].
[17] V. V. Anisovich, B. Ch. Metsch, H. R. Petry, and A. V. Sarantsev, to be published in Z. Phys. A.
[18] V. V. Anisovich, Yad. Fiz. **31**, 859 (1980) [Sov. J. Nucl. Phys. **31**, 444 (1980)].
[19] A. Monohar and A. Georgi, Nucl. Phys. B **234**, 189 (1984).
[20] J. Weinstein and N. Isgur, Phys. Rev. D **27**, 588 (1983); **41**, 2236 (1990).
[21] T. Barnes and E. S. Swanson, Phys. Rev. D **46**, 131 (1992).
[22] S. V. Gerasimov, Yad. Fiz. **29**, 513 (1979) [Sov. J. Nucl. Phys. **29**, 259 (1979)]; **32**, 304 (1980) [**32**, 156 (1980)].
[23] D. Morgan, Nucl. Phys. A **543**, 632 (1992).
[24] D. Morgan and M. R. Pennington, Phys. Rev. D **48**, 1185 (1993). **46**, 131 (1992).
[25] N. Törnqvist, Phys. Rev. Lett. **67**, 556 (1991).
[26] K. Dooley, E. S. Swanson, and T. Barnes, Phys. Lett. B **275**, 478 (1992).
[27] H. Herschbach, Phys. Rev. D **47**, 3027 (1993).
[28] W. Bürger, M. Faber, H. Markum, and M. Müller, Phys. Rev. D **47**, 3034 (1993).
[29] D. E. Kahana, K. M. Maung, and J. W. Norbury, Phys. Rev. D **48**, 3408 (1993).
[30] C. Semey and R. Ceuleneer, Phys. Rev. D **48**, 4361 (1993).
[31] A. De Rujula, H. Georgi, and S. L. Glashow, Phys. Rev. D **12**, 147 (1975).
[32] E. Ma, Phys. Rev. D **17**, 623 (1978).
[33] V. V. Anisovich *et al.*, Phys. Lett. B **323**, 233 (1994).
[34] V. V. Anisovich, D. V. Bugg, A. V. Sarantsev, and B. S. Zou, Phys. Rev. D **50**, 1972 (1994).
[35] Particle Data Group, Phys. Rev. D **50** (1994).
[36] Y. Nambu and G. Jona-Lasinio, Phys. Rev. **122**, 345 (1961); **124**, 246 (1961).
[37] V. Bernard and U. Meissner, Phys. Lett. B **266**, 403 (1991).
[38] M. K. Volkov, Fiz. Elem. Chastits At. Yadra **17**, 433 (1986) [Sov. J. Part Nucl. **17**, 186 (1986)].
[39] P. Mackenzie, Nucl. Phys. B (Proc. Suppl.) **30**, 35 (1993).
[40] S. Sharpe, Nucl. Phys. B (Proc. Suppl.) **30**, 213 (1993).
[41] C. Davies (UKQCD Collaboration), UKQCD Review, International Conference on Nuclear and Particle Physics, 1993, edited by I. J. D. MacGregor and A. T. Doyle (Institute of Physics Publishing, Bristol, England).
[42] S. M. Gerasyuta *et al.*, Yad. Fiz. **53**, 1397 (1991) [Sov. J. Nucl. Phys. **53**, 864 (1991)].
[43] M. Roos and N. Törnqvist, Z. Phys. C **5**, 205 (1980).
[44] N. Törnqvist, Nucl. Phys. B **203**, 268 (1982).
[45] V. V. Anisovich, M. N. Kobrinsky, D. I. Melikhov, and A. V. Sarantsev, Nucl. Phys. A **544**, 747 (1992).
[46] V. V. Anisovich, D. V. Bugg, and A. V. Sarantsev, Nucl. Phys. A **501**, 501 (1992).
[47] V. V. Anisovich, D. I. Melikhov, B. Ch. Metsch, and H. R. Petry, Nucl. Phys. A **563**, 549 (1993).
[48] S. M. Flatté, Phys. Lett. B **63**, 224 (1976).
[49] B. Hyams *et al.*, Nucl. Phys. B **64**, 134 (1973).
[50] D. Aston *et al.*, Nucl. Phys. B **296**, 493 (1988).
[51] P. Estabrooks *et al.*, Nucl. Phys. B **133**, 491 (1978).
[52] C. D. Froggat and J. L. Petersen, Nucl. Phys. B **129**, 89 (1977).
[53] S. D. Protopopescu *et al.*, Phys. Rev. D **7**, 1280 (1973).

Translated by Julian B. Barbour